https://doi.org/10.1016/j.ces.2020.115773

Model Reductions for Multiscale Stochastic Optimization of Cooling Water System Equipped with Closed Wet Cooling Towers

Qiping Zhu, Bingjian Zhang, Qinglin Chen, Chang He*
School of Materials Science and Engineering, Guangdong Engineering Centre for Petrochemical Energy Conservation, Sun Yat-sen University, Guangzhou, 510275, China.

Dominic C.Y.Foo
Department of Chemical & Environmental Engineering/Centre of Excellence for Green Technologies, University of Nottingham, 43500 Semenyih, Selangor, Malaysia

Jingzheng Ren
Department of Industrial and Systems Engineering, The Hong Kong Polytechnic University, Hong Kong Special Administrative Region, China

Haoshui Yu
MIT Energy Initiative, Massachusetts Institute of Technology, 77 Massachusetts Avenue, Cambridge, MA, 02139, USA

*Corresponding authors: Chang He, E-mail addresses: hechang6@mail.sysu.edu.cn.

Abstract

Incorporation of closed wet cooling tower (CWCT) in the existing circulating water system has been recognized as a viable path to reduce industrial water consumption. This paper introduces a specifically tailored framework based on model reductions for multiscale optimization of CWCT-based cooling water system considering environmental variations. An optimal design of experiment is performed for accurate approximation of the multivariate probability distributions by generating a finite set of samples over the input space. The probability distributions are propagated via multi-sample CFD simulations for constructing the physics-based and data-driven reduced models of CWCTs. Based on the developed reduced models, a multi-scale optimization model is proposed for performing integrated design and management of CWCTs and cooling water system. It employs sampling-based stochastic programming and the heterogeneous integration of reduced models of CWCTs and other shortcut models. Finally, the performance of the proposed approach is illustrated through its comparison with a deterministic approach.

Keywords: Model reduction; Cooling water system; Design of experiment; Multi-scale optimization; Design

1. Introduction

Reducing freshwater consumption is critical to the sustainable development of process industry due to growing water scarcity. In the petrochemical and thermo-electric sectors, circulating water losses, especially the evaporation loss from open wet cooling towers, are the main contributors to the demand for freshwater during plant operation. Incorporation of emerging *closed wet cooling towers* (CWCTs) in the existing cooling water system has been recognized as the viable mid/long-term path to achieving process intensification due to their remarkable advantages in water-saving, plume reduction, and non-pollution to the process water.[1-3] Nevertheless, it remains a challenging problem at the device-scale to gain a better understanding of the CWCT, as the latter is characterized by highly complex counter-current interactions between multi-phase flow dynamics and film heat transfer processes. At the system-scale, on the other hand, the CWCTs which act as the core of the closed-loop cooling water system remain very sensitive, or even vulnerable to the changes in operating and weather conditions. Multiple types of uncertainties involved in cooling water systems add more complexity and instability in iterative computation. Thus, it is crucial to develop high-fidelity CWCT models and to interactively leverage the developed models in the multi-scale design and optimization of cooling water systems with explicit consideration of uncertainties.

The acquisition of a better understanding of CWCT models is typically approached by carrying out extensive mathematical studies on empirical correlation-based models,[3-5] or detailed full-order models (FOMs).[2] The former models basically result from energy and mass balances that consist of lumped parameters description with a number of ideal assumptions. These empirical findings neither account for complex fluid dynamic and transport effects, nor do they account for specific CWCTs that take place at broader length scales, hence leading to limited applications.[6-8] In order to obtain more realistic

results, FOMs constructed by multi-phase CFD modelling or mathematical programming have been widely used to describe the underlying heat-mass transfer behaviour which occurs outside the tube bundle of CWCTs[9, 10]. Note that the CFD models implemented in FLUENT software tracks the interactions and spatial movement of each particle characterized by computationally intractable equations, such as distributed partial differential and algebraic equations (PDAEs). Thus, the benefits of FOMs must be weighed against the time necessary to solve them, which is a major cost driver and impedes developing better processes. For example, a single task of CFD simulation normally takes 30 ~70 CPU hours for 3-D CWCTs using Reynolds Average Navier-Stokes equations due to informative models and iterative computation. Besides, data interface and transfer issues lead to poor integration of CFD models with flowsheet simulation software, preventing information exchange for multi-scale simulation. These issues become more critical as the integrated models are encountered in an equation-oriented optimization task because a large number of recourses to the CFD models have to be executed before converging to optimum FOMs. The CPU time and memory costs increase exponentially, which can even lead to a combinatorial explosion on the computation burden if an effective strategy is not applied.

To solve the above-mentioned problems, it is imperative to construct a more tractable model as an alternative for the computationally-expensive FOMs in numerical simulations. Reduced-order modelling (ROM)[11-13] is a technique that involves small degrees of freedom, which reproduces the behaviour of an actual physical system or a reference FOM without loss of fidelity.[14] Over the past decades, the benefits of ROMs have been evaluated for many chemical processes, e.g. pressure swing adsorption[15], solid handling[16-18], fluidized bed adsorption[12], complex distillation[19] , oil and gas[20-22] , and fluids[23], etc. Besides, recent work explores the application of ROMs in multi-scale integration by

mapping process outputs to input variables using a meta-modelling approach such as polynomial response[24, 25], artificial neural network[11, 26, 27], and Kriging interpolation[19, 28, 29]. For example, it becomes essential to wrap reduced models (RMs) to fit multi-scale models for material design and detailed unit operations (CFD, FOMs, PDAEs) into the overall process system. This multi-scale integration further enables researchers to simultaneously consider the heterogeneous collection of micro- and macro-scale model and the optimization of these integrated models, e.g. supply chain system[30], coal gasification[27], and other process systems[31-33], using efficient non-linear programming techniques[34-36]. General information about ROM-based multi-scale process optimization can be found in the reviews by Floudas et al.[37] and Biegler.[38] To date, there are quite few studies focusing on the ROMs of cooling towers, such as those by Gao et al.[39], Wei et al.[40], and Qasim et al.[41]. However, most of the existing studies are restricted to the device-scale and only rely on deterministic conditions. The operation of cooling towers is directly affected by the fluctuating atmospheric conditions. As aforementioned, multiple types of uncertainties on weather conditions could strongly hamper the design and operation of the CWCTs and cooling tower system as the closed-loop system. Situation is worse especially in extreme cases, such as over-heated or over-humid weather which usually happen during summer. In this case, there may be abnormal operations in which the cooling targets of the cooling tower system cannot be achieved, due to relatively small evaporation on the surface of coil tubes. Existing studies typically assume that the weather conditions are perfectly known or even fixed in advanced without seasonal variability, leading to an over-optimistic design and/or underestimation of the negative impacts on the performance of the cooling tower systems. This entails the need to properly characterize the uncertainties in the construction of reduced models for CWCTs.

Considering the aforementioned issues, this work seeks to develop an integrated framework for

model reduction and multi-scale optimization for a cooling water system equipped with CWCTs, with consideration of uncertain environmental parameters. For the first step, it proposes a model reduction methodology to process the input data and generate bi-level RMs for CWCTs by implementing four statistical steps, i.e. optimal design of experiment, multi-sample CFD simulation, reduced models construction, and model evaluation. In order to fully accommodate the diverse nature of weather variability, an optimal design of experiment is performed for accurate approximation of the multi-variate probability distributions by generating a finite set of Hammersley points (samples) over the entire input space. These samples are performed by rigorous CFD simulation to extract a series of input-output data for constructing the bi-level RMs which include the physics-based RM and data-driven RMs. The developed RM is embedded within the sampling-based multi-scale models for stochastic optimization of CWCTs and cooling water systems. The applicability and advantage of the proposed framework is illustrated and compared with the deterministic approach on the cost and freshwater consumption through an industrial example.

2. Full-Scale Physical Model of CWCTs

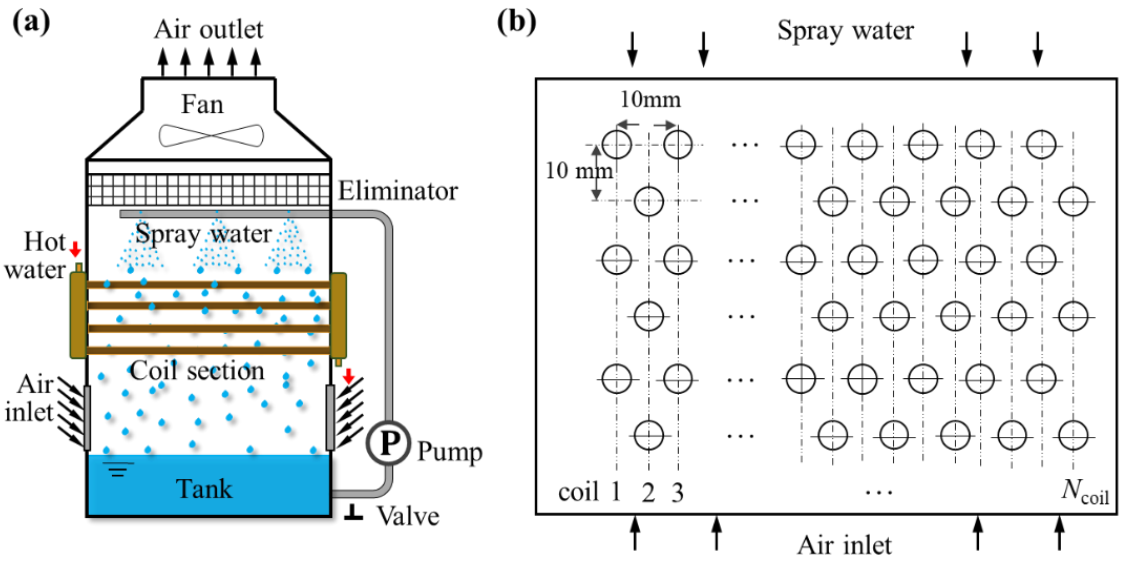

Fig. 1. (a) Sketch of the CWCT set-up and (b) cross-section of the tube bundle

The physical model of CWCTs investigated in this study is based on a bench-scale experimental set-up[2] with parallel counter-flow construction. As shown in **Fig. 1**(a), the ambient air flows upward and traverses the outer wall of the tube bundle by means of the intake fan in counter-current flow with the spray water. Meanwhile, the hot circulating water pumped from the main tube is evenly divided and distributed across the serpentine tubes inside the tower casing, in which its sensible heat is indirectly absorbed by film evaporation and upward air flow outside the tube bundle. The heat and mass transfer processes of water film are mainly sustained by the joint effect of counter-current spray water and ambient air. A small proportion of spray water diffuses together with the upward airflow due to evaporation, and the remaining portion leaving the water film is collected in a water tank and finally returns to the top nozzles through the spray pump. Thus, the circulating water basically relies on the film evaporation to achieve the required cooling target, such as temperature drop and heat dissipation.

In this work, we focus on heat and mass transfer processes of the water film outside the tube bundle of CWCTs, which are simulated by a two-dimensional (2-D) CFD model of flow, temperature, and pressure fields. The cross-section of the tube bundle is in a triangular arrangement and the arbitrary adjacent tubes in each row have the same centerline spacing, as shown in **Fig. 1**(b). In order to simplify the calculation, several assumptions are made as follows: (1) the outer wall of the coil tubes have no slips; (2) the circulating water and inlet air are both incompressible fluids; (3) the surface of the coil tubes is evenly covered by water film, while the air flow and spray water are uniformly distributed throughout the tower; (4) the temperature of the water film is equal to the average temperature of circulating water; and (5) the thermal radiation between the tower and the surroundings is neglected. Besides, note that a commercial scale CWCT has a relatively small cooling capacity (e.g., inlet circulating water flow rate<500 m^3/h). It is approximated by taking advantage of the fact that several

parts, such as coil tubes, are geometrically standardized using certain a finite set of standard diameters and thicknesses. In 2-D modelling, the cooling capacity can be expanded approximately in proportion to the number of tubes in order to meet the actual requirements.

In CWCTs, the complex heat and mass transfer processes outside the tubes can be mathematically described by large-scale PDAEs that are constructed from mass and energy conservation and hydro-dynamic equations. These equations can be written in a general transport equation form as presented in Eqs. (1-14). Among them, the Navier-Stokes and energy conservation equations are as follows:

$$\frac{\partial \rho}{\partial t} + \nabla \cdot (\rho \vec{v}) = S_m \tag{1}$$

$$\frac{\partial}{\partial t}(\rho \vec{v}) + \nabla \cdot (\rho \vec{v}\vec{v}) = -\nabla P_{sp} + \nabla \cdot (\tilde{\tau}) + \rho \vec{g} + \vec{F}b \tag{2}$$

$$\frac{\partial}{\partial t}(\rho E) + \nabla \left(\vec{v} \left(\rho E + P_{sp} \right) \right) = \nabla \left(kc_{eff} \nabla T - \sum_{js} h_{js} D_{js} + \left(\tilde{\tau}_{eff} \cdot \vec{v} \right) \right) + S_h \tag{3}$$

where ρ and v are density and velocity; S_m is the mass added to the continuous phase from the dispersed second phase; P_{sp} and $\tilde{\tau}$ are the static pressure and the stress tensor; $\rho \vec{g}$ and $\vec{F}b$ are the gravitational body and external body forces; E and kc_{eff} are the energy and effective conductivity; h_{js} and D_{js} are the sensible enthalpy and diffusion flux of species *js*, respectively; $\tilde{\tau}_{eff}$ is the effective stress tensor; S_h is a user-defined source term. In addition, the first three terms on the right-hand side of Eq. (3) represent energy transfer due to conduction, species diffusion, and viscous dissipation, respectively.

This work employs the Eulerian-Lagrangian approach[42-44] for the numerical calculation of the dynamics of multi-phase flows. The fluid phase of air is treated as a continuum by solving the Navier-Stokes equations, while the spray water used as a dispersed phase is solved by tracking a large number of particles or droplets through the calculated flow field. The dispersed phase can exchange momentum, mass, and energy with the fluid phase. The trajectory of a particle or droplet of the dispersed phase is

predicted by integrating the force balance on the particle. This force balance equates the particle inertia with the forces acting on the particle, which is written as follows:

$$\frac{dv_p}{dt} = \frac{v_f - v_p}{\varsigma} + \frac{\vec{g}(\rho_p - \rho_f)}{\rho_p} + \vec{F} \tag{4}$$

$$\varsigma = \frac{\rho_p d_p^2}{18\mu_f} \frac{24}{C_d \,\mathrm{Re}} \tag{5}$$

$$\mathrm{Re} = \frac{\rho_f d_p \left| v_p - v_f \right|}{\mu_f} \tag{6}$$

where v_f, μ_f and ρ_f are the velocity, molecular viscosity and density of the fluid, respectively; v_p, ρ_p and d_p are the velocity, density and diameter of the particle, respectively; $(v_f\text{-}v_p)/\zeta$ is the drag force per unit particle mass, *Re* is the relative Reynolds number.

According to the previous investigations[2, 45], the realizable *k*-*ε* model that presents a sufficient adaptation with the physics of flow turbulence is applied to model the turbulent flow outside the tubes in the tower. Based on the general form of the transport equation, the turbulence kinetic energy *ke*, and its rate of dissipation *ε*, are obtained from the realizable *k*-*ε* model equations, which are expressed as:

$$\frac{\partial}{\partial t}(\rho ke) + \frac{\partial}{\partial x_{is}}(\rho ke u_{is}) = \frac{\partial}{\partial x_{js}}\left[\left(\mu + \frac{\mu_t}{C_{ke}}\right)\frac{\partial ke}{\partial x_{js}}\right] + Gk + Gb - \rho\varepsilon - yr_M + S_{ke} \tag{7}$$

$$\frac{\partial}{\partial t}(\rho\varepsilon) + \frac{\partial}{\partial x_{is}}(\rho\varepsilon) = \frac{\partial}{\partial x_{js}}\left[\left(\mu + \frac{\mu_t}{C_{\varepsilon}}\right)\frac{\partial \varepsilon}{\partial x_{js}}\right] + \rho C_1 S\varepsilon - \rho C_2 \frac{\varepsilon^2}{ke + \sqrt{v\varepsilon}} + C_{1\varepsilon}\frac{\varepsilon}{ke} C_{3\varepsilon} Gb + S_{\varepsilon} \tag{8}$$

where *Gk* and *Gb* represent the generation of turbulent kinetic energy due to the mean velocity gradients and buoyancy; yr_M is the contribution of the fluctuating dilatation in compressible turbulence to the overall dissipation rate; C_2 and $C_{1\varepsilon}$ are constants; C_{ke} and C_{ε} are the turbulent Prandtl numbers for parameters *ke* and *ε*.

The mixture special transport model is employed to calculate the concentration of different species in the CWCT, and the convection-diffusion equation used to solve these given by Eq. (9).

$$\frac{\partial}{\partial t}\left(\rho fm_{is}\right)+\nabla\cdot\left(\rho\vec{v}y_{is}\right)=-\nabla\cdot D_{is}+R_{is}+S_{is} \tag{9}$$

$$D_{is}=-\left(\rho D_{m,is}+\frac{\mu_t}{Sc_t}\right)\nabla y_i-D_{T,is}\frac{\nabla T}{T} \tag{10}$$

where fm_{is}, R_{is}, $D_{m,is}$ and $D_{T,is}$ are the mass fraction, net rate, mass diffusion, and thermal diffusion coefficients for species *is*, respectively; Sc_t is the turbulent Schmidt number and the default is 0.7.

The Eulerian wall film model coupled with the mixture species transport model is used to calculate phase changes between film liquid and gas vapour. The rate of phase change is governed by:

$$\dot{m}_{phase}=\frac{\left(\rho_{mix}D_{vap}/WD\right)}{\rho_{mix}D_{vap}/WD+C_{phase}}C_{phase}\left(fm_{sat}-fm_{vap}\right) \tag{11}$$

$$fm_{sat}=\frac{P_{sat}T}{P_{mix}}\frac{M_{vap}}{M_{mix}} \tag{12}$$

where ρ_{mix} is the density of the gas mixture; D_{vap} is the mass diffusivity of the vapor species; *WD* is the cell-centre-to wall distance; C_{phase} is the phase change constant; fm_{sat} and fm_{vap} are the mass fractions of the saturation species and vapour species, respectively. In addition, P_{sat} and P_{mix} are the absolute pressure of the saturation species and gas mixture, M_{vap} and M_{mix} are the molecular weights of the vapour species and mixture, respectively.

The droplet temperature is updated according to the energy balance shown in Eq. (13) that relates the sensible heat change between the droplet to the convective and latent heat transfer between the droplet and the continuous phase:

$$m_p c_{pp}\frac{dT_p}{dt}=htA_p\left(T_\infty-T_p\right)-\frac{dm_p}{dt}Q_{lh}-A_p\zeta_p C_{SB}T_p^4 \tag{13}$$

where c_{pp} is the droplet heat capacity, *ht* is the convective heat transfer coefficient, T_∞ and T_p are the temperatures of the continuous phase and droplet, dm_p/dt and Q_{lh} are the evaporation rate and latent heat, C_{SB} is the Stefan-Boltzmann constant.

3. RM-based Multi-Scale Optimization Framework

In **Fig. 2**, an integrated framework based on model reduction methodology was introduced; the framework is capable of considering multi-scale optimization of the cooling water systems installed with CWCTs. For better implementation of the RMs, the entire input space (input variables, matrix **X**) that contains three sets of variables, i.e. operating variables $\mathbf{X}^{(1)}$, uncertain variables $\mathbf{X}^{(2)}$ and design variables $\mathbf{X}^{(3)}$ must be specified (see values in

Table 1). As shown in **Fig. 2**(a), an optimal design of experiment (DoE) is performed for accurately approximating the multi-variate probability distributions and generate a finite set of homogeneous samples over the entire input space (a-1). Next, the multi-variate probability distributions of generated samples are propagated by executing the rigorous CFD simulation of CWCTs for each of the samples (a-2). The results of both the state space (distributed variables in the fluid field, matrix **Z**) and output space (output variables, matrix **Y**) are recorded after convergence. These two types of recorded results, together with the input variables are used to construct the physics-based and data-driven RMs (a-3), respectively, as detailed in Section 4.

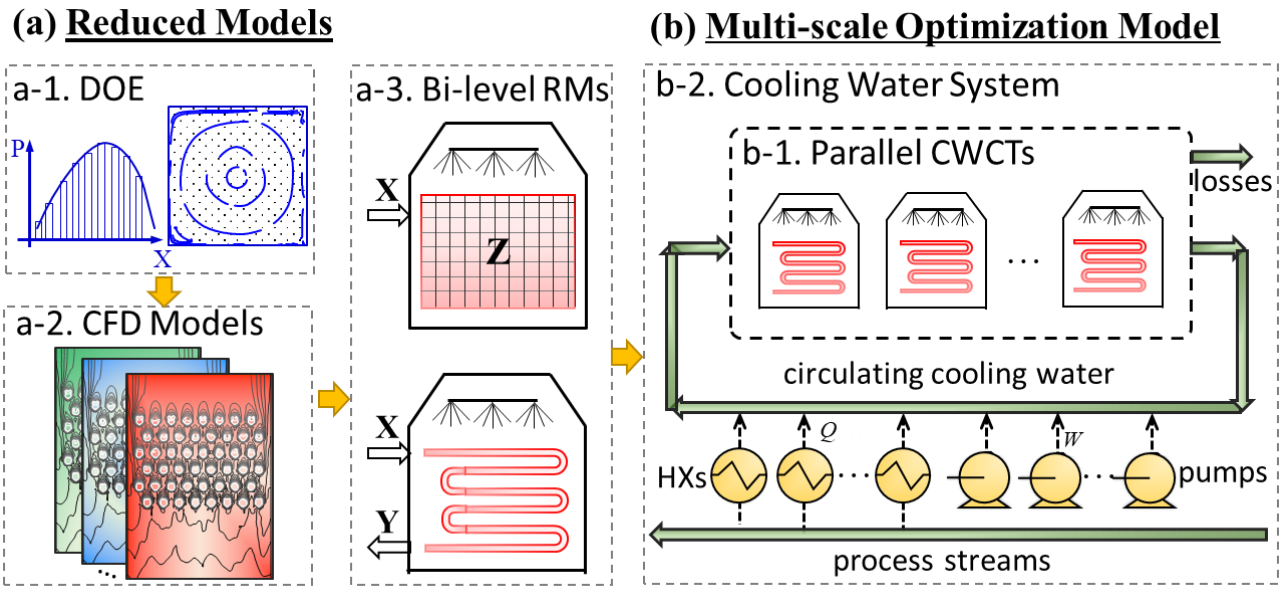

Fig. 2. Schematic description of the RM-based multi-scale optimization framework.

Based on the developed bi-level RMs, a multi-scale optimization model is further proposed for performing integrated design and management of the CWCTs and cooling water system (see **Fig. 2(b)**). It employs sampling-based stochastic programming and heterogeneous integration of unit-specific shortcut models (heat exchangers and pumps) and multi-scale models of CWCTs. Note that, due to the independence of stochastic programming on the samples, the size of the multi-scale design problem

may increase exponentially as the number of samples increases. To remove this barrier, another DoE is implemented for efficient realization of uncertain variable $\mathbf{X}^{(2)}$. The discrete realizations are passed to the stochastic optimization programming model of the cooling water system. The detailed model formulations for the stochastic optimization model are provided in Section 5.

4. Model Reduction Methodology

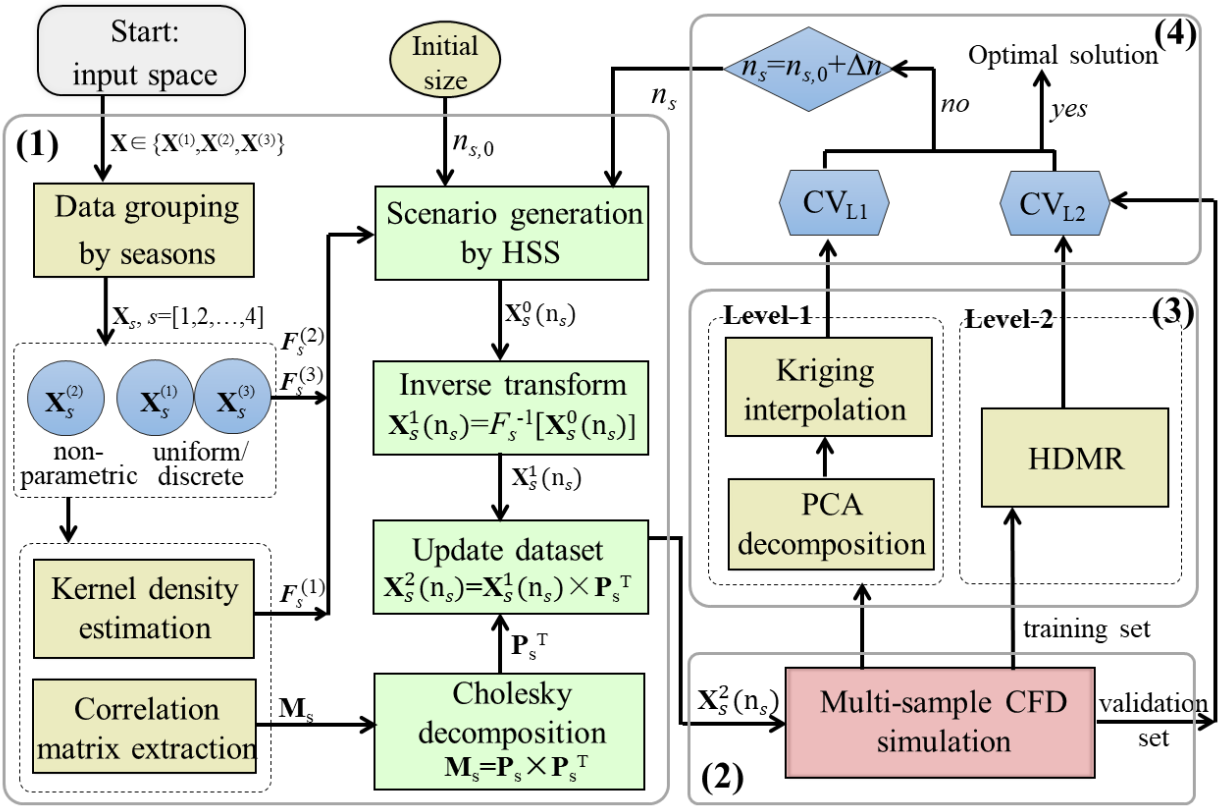

Fig. 3. The proposed model reduction methodology.

Fig. 3 shows the model reduction methodology to process input data and to generate bi-level RMs for the CWCTs. It consists of four statistical steps (1) optimal DoE, (2) multi-sample CFD simulation, (3) reduced models construction and (4) model evaluation.

4.1 Optimal design of experiments

DoE is a well-suited approach to reduce resources and time, as it can maximize the amount of

process information obtained from a finite size of calculations by properly selecting experimental points. As seen in **Fig. 3**(a), it starts with a parameter characterization for input space to obtain the probability density functions (PDFs) of multi-variate. Herein, the operating variables $\mathbf{X}^{(1)}$=[v^a, m^{sw}, T^{sw}, T^{cw}, m^{cw}] can be directly characterized by uniform distributions with known bounds according to the operating constraints, while the design variables $\mathbf{X}^{(3)}$=[d^{tube}, N^{tube}] are discrete points provided by the equipment manufacturer. Besides, note that the uncertain variables $\mathbf{X}^{(2)}$= [T^{db}, φ^{rh}], depending on the actual weather conditions normally fall into distinct temperature-intervals in different seasons and thus are hard to be described by any standard parametric probability distribution models like Normal distribution. Thus, the original data in the input space requires pretreatment and segregation into four distinct groups by seasons $\mathbf{X}_s^{(2)}$, $s \in \{1,\ldots,4\}$. These grouped datasets are then processed by the Gaussian Kernel density estimation stated in Eq. (14) that provides a non-parametric alternative to smooth and approximate the cumulative distribution function (CDF, F_s) of the uncertain variables.

$$F_s^{(1)}(x) = \frac{1}{n_s \sigma_s}\left(\frac{4}{3n_s}\right)^{-1/5} \sum_{i=1}^{n_s} G\left[x - \mathrm{X}_s^{(2)}(i)\right] \quad s \in \{1,...,4\} \tag{14}$$

$$G(x) = \int_{-\infty}^{x} \frac{1}{\sqrt{2\pi}} \exp\left(-\frac{1}{2}t^2\right) \mathrm{d}t \tag{15}$$

where σ_s and n_s are the variance and size of $\mathbf{X}_s^{(2)}$.

Table 1. The input space for the RM construction

Input variables	Symbol	Units	Specification
Operating variables	$\mathbf{X}^{(1)}$		
velocity of inlet air	v^a	m/s	U(1.0, 2.5)
mass flowrate of spray water	m^{sw}	kg/s	U(0, 1.0)
temperature of spray water	T^{sw}	K	U(285, 310)
volume flow rate of circulating water	m^{cw}	m^3/h	U(0, 500)
temperature of inlet circulating water	T^{cw}	K	U(313, 330)
Uncertain variables	$\mathbf{X}^{(2)}$		
dry bulb temperature of inlet air	T^{db}	K	uncertain distribution
relative humidity of inlet air	φ^{rh}	%	uncertain distribution
Design variables	$\mathbf{X}^{(3)}$		
inner diameter of tube	d^{tube}	m	{0.01, 0.02, …, 0.1}
numbers of tube bundle	N^{tube}	/	{200, 201, …, 1000}

Once all input variables are characterized, the developed probability distribution models are discretized into a finite set of distinct samples for performing stochastic CFD simulation by means of sampling. In this study, an efficient sampling technique, Hammersley sequence sampling (HSS) based on Hammersley points[46, 47] for evenly placing the sample points on a k-dimensional hypercube is employed to ensure that the sample set is more representative of the original data. Note that the uncertain variables of interest have a positive symmetric correlation, e.g. the profile of saturated humidity generally has an evident decrease as the temperature is reduced from warm to cold seasons. This would badly distort the actual multi-variate distribution as well as the uniform property of the sampled points over the input space. Thus, the sampled set $\mathbf{X}_s^0$ should be rearranged via the implementation of rank correlations to guarantee the independence of the dataset and to obtain almost the same probability distribution for each variable with the historical data. This work utilizes the Pearson correlation coefficient (PCC, ρ) to define the correlation structure $\mathbf{M}_s$ among all uncertain

variables of interest. At this point, $\mathbf{X}_s^0$ is mapped to the inverse CDF, resulting in an inverse transformed dataset $\mathbf{X}_s^1$. Multiplying dataset $\mathbf{X}_s^1$ with the lower triangular matrix $\mathbf{P}_s^{\mathrm{T}}$ (by Cholesky decomposition[48] of $\mathbf{M}_s$, $\mathbf{M}_s=\mathbf{P}_s\times\mathbf{P}_s^{\mathrm{T}}$), we can obtain $\mathbf{X}_s^2$ as the solution of DoE.

$$\rho_s(i,j)=\frac{cov\left[\mathrm{X}_s^{(2)}(i),\ \mathrm{X}_s^{(2)}(j)\right]}{\sigma\left[\mathrm{X}_s^{(2)}(i)\right]\sigma\left[\mathrm{X}_s^{(2)}(j)\right]} \qquad \forall i\neq j\in\left\{T^{db},T^{dw},\varphi^{rh}\right\};\ \ s\in\{1,2,...,4\} \tag{16}$$

$$\mathbf{M}_s=\begin{bmatrix}\rho_s(1,1) & \rho_s(1,2) & \rho_s(1,3)\\ \rho_s(2,1) & \rho_s(2,2) & \rho_s(2,3)\\ \rho_s(3,1) & \rho_s(3,2) & \rho_s(3,3)\end{bmatrix} \tag{17}$$

4.2 Multi-sample CFD simulation

In order to obtain the datasets for the development of RMs, the discretized PDAEs for CWCTs are solved by using FLUENT software for each of the samples. Note that, there are four groups of input-output data mapping by seasons. For each season group, the process has *n* inputs and *m* outputs, and with *s* state variables (temperature, pressure, and velocity, etc.) that are bounded by the geometry of equipment and monitored within the process in a total of *p* discretized elements.

The process geometry of the tube bundle section shown in **Fig. 1**(b), firstly drawn using the Design Modeler package, is based on the standard diameter and length listed in

Table 1. The generated preliminary sketch is meshed to adequately capture the change of fluids using the Meshing package. Note that the meshes near to the tube walls are refined to improve the model accuracy. Besides, the element size is smoothly stretched to ensure an accurate resolution of the high gradient regions of the fluid fields. The quality of the mesh structure is measured by the skewness value which should be less than the required level (1-inacceptable, 0-excellent). Next, multiple CFD simulations are performed on the meshed geometry to calculate the coupled heat and mass transfer, as well as the mass and energy balances of PDAEs. In particular, the Eulerian-Lagrangian modelling approach is applied whereby the air phase is treated as continuous and the spray water particles are handled using the discrete phase model. The particle trajectories, along with mass and energy transfer to the particles, are computed with a Lagrangian formulation. The air-water two-phase flow employs the realizable k-ε model. The governing equations with boundaries are solved by the finite volume method, and the convective terms in governing equations are discretized by the QUICK scheme with second-order precision.

4.3 Reduced models construction

4.3.1 Level 1: Physics-based RM

Step 1: Singular value decomposition method

The principal component analysis (PCA) decomposition method based on SVD can map a vector from n-dimensional space to a k-dimensional space ($k<<n$) by transforming the snapshot data to a new orthogonal coordinate system without significant loss of information. The essence of SVD is to find a set of orthogonal bases, which is still orthogonal after transformation. Assuming $\mathbf{Z}$ is a $m\times n$ snapshot matrix, which represents all the output variables in the nodes of the mesh at a special state like temperature and velocity fields. The matrix $\mathbf{Z}$ with rank order k maps a set of orthogonal basis $\mathbf{V}=[v_1,$

v_2,…, v_n] to another set of orthogonal basis **ZV** that must be satisfy the conditions $v_a \cdot v_b = v_a^{\mathrm{T}} v_b = 0$ and $\mathbf{Z}v_a \cdot \mathbf{Z}v_b = (\mathbf{Z}v_a)^{\mathrm{T}}\mathbf{Z}v_b = v_a^{\mathrm{T}}\mathbf{Z}^{\mathrm{T}}\mathbf{Z}v_b = 0$, where $a \neq b = [1, 2, \ldots, n]$. Since $\mathbf{Z}^{\mathbf{T}}\mathbf{Z}$ is a symmetric matrix, its Eigenvectors of different Eigenvalues are orthogonal to each other and the orthogonal basis **V** can be set the Eigenvectors of $\mathbf{Z}^{\mathbf{T}}\mathbf{Z}$, $|\mathbf{V}| = k = rank(\mathbf{Z})$. Thus, there is $v_a^{T}\mathbf{Z}^{\mathrm{T}}\mathbf{Z}v_b = v_a^{\mathrm{T}}\lambda_b v_b = \lambda_b v_a \cdot v_b = 0$, where $1 \leq a, b \leq k$, $a \neq b$. The orthogonal basis **ZV** can be unitized as $u_a = \mathbf{Z}v_a / |\mathbf{Z}v_a| = \lambda_a^{-1/2}\mathbf{Z}v_a$, where $\mathbf{Z}v_a = \sigma_a u_a$, $\sigma_a = \lambda_a^{-1/2}$, $0 \leq a \leq k$ and σ_a is the singular value. The up-dated orthogonal basis [u_1, u_2,…, u_k] and [v_1, v_2,…, v_k] needs to be extended to another orthogonal basis **U**=[u_1, u_2,…, u_m] if $k<m$, and **V**=[v_1, v_2,…, v_n] if $k<n$, respectively. In addition, the dataset [v_{k+1}, v_{k+2},…, v_n] can be set to the null space of **Z** ($\mathbf{Z}\mathbf{V}_a = 0$, $a>k$, $\sigma_a = 0$). Finally, matrix **Z** is decomposed into three matrixes after eliminating zero.

$$\mathbf{Z} = \mathbf{U}\mathbf{\Sigma}\mathbf{V}^{T} \tag{18}$$

where $\mathbf{\Sigma} = \mathrm{diag}\{\sigma_1, \ldots, \sigma_k, 0\}$. Note that σ declines rapidly with the rank order of $\sigma_1 \geq \sigma_2 \ldots \geq \sigma_k$, in most cases, the sum of the top 10% of σ can account for more than 95% of the total singular values. Reducing **Z** to rank k resulting from this cutoff criterion, the reduced-order dataset is obtained as given by:

$$\mathbf{Z} \approx \mathbf{Z}^{(k)} = \mathbf{U}^{(k)}\mathbf{\Sigma}^{(k)}(\mathbf{V}^{(k)})^{T} \tag{19}$$

where the superscript (k) indicates that the first k columns are taken from the original matrix to formulate a new matrix and k is far less than m or n. Then, the matrix **Z** can be expressed as its principal component (PC) matrix (δ) and score matrix (Φ).

$$\mathbf{Z} = \delta\Phi \tag{20}$$

where $\delta = \mathbf{U}^{(k)}$ is a $m \times k$ matrix; $\Phi = \mathbf{\Sigma}^{(k)}(\mathbf{V}^{(k)})^{T}$ is a $k \times n$ diagonal matrix.

Step 2: Kriging interpolation

The PCs are unchanged for any given input variables **X** because they represent the coordinate in the transformed system via PCA decomposition of the original dataset. For any input variables **X** restricted in the domain, it only needs to obtain the score Φ to calculate the output variables **Z** through

the linear correlation defined in Eq. (20). Note that the only varying components in this equation are the score Φ obtained from PCA with a potential correlation between Φ and **X**. Additional functions between them can be built with Kriging interpolation according to the complexity of the CFD model.

The Kriging predictor Φ(**X**) consists of polynomial term *pt*(**X**) and residual term *rt*(**X**), which can be used to substitute for the PDAEs model. Due to the stochastic assumption in the Kriging interpolation, the error in the predicted value is also a function of the input variables **X**.

$$\Phi(\mathbf{X}) = pt(\mathbf{X}) + rt(\mathbf{X}) \tag{21}$$

where *pt*(**X**) is a constant $\boldsymbol{\mu}$, *rt*(**X**) is a stochastic Gaussian process denoting the uncertainty on the mean of Φ(**X**).

To keep the predictor unbiased, the expected value of the residual term *rt*(**X**) is zero, $E[rt(\mathbf{X})]=0$. The covariance between points ($\mathbf{X}_{l1}$, $\mathbf{X}_{l2}$) of this term can be calculated by $cov[rt(\mathbf{X}_{l1}, \mathbf{X}_{l2})]=\boldsymbol{\sigma}^2 \Psi(\mathbf{X}_{l1}, \mathbf{X}_{l2})$, where $\boldsymbol{\sigma}^2$ is the process variance, $\Psi(\mathbf{X}_{l1}, \mathbf{X}_{l2})$ is the spatial correlation function as follows:

$$\psi\left(\mathbf{X}_{l1},\ \mathbf{X}_{l2}\right) = \exp\left[-d\left(\mathbf{X}_{l1},\ \mathbf{X}_{l2}\right)\right] \tag{22}$$

$$\widehat{\psi}\left(\mathbf{X}_{l1},\ \mathbf{X}\right) = \exp\left[-d\left(\mathbf{X}_{l1},\ \mathbf{X}\right)\right] \tag{23}$$

$$d\left(\mathbf{X}_{l1},\ \mathbf{X}_{l2}\right) = \prod_{h=1}^{g} \exp\left[-\theta_h \left(\mathbf{X}_{l,h} - \mathbf{X}_{l2,h}\right)^{p_h}\right],\quad \forall h \in \{1,...,g\} \tag{24}$$

where the Gauss correlation is employed due to the continuously differentiable of the underlying phenomenon; $\boldsymbol{\theta}$ is the Kriging regression parameter; $\boldsymbol{p}_h$ is the smoothness parameter which is equal to 2 and provides a smooth infinitely differentiable correlation function. The values of parameters ($\boldsymbol{\mu}$, $\boldsymbol{\sigma}^2$, $\boldsymbol{\theta}$) are fit by applying the maximum likelihood parameter estimation method, and the estimations of $\boldsymbol{\mu}$ and $\boldsymbol{\sigma}^2$ are $\boldsymbol{\mu}=(1^T\Psi^{-1}\mathbf{Z})/(1^T\Psi^{-1}1)$ and $\boldsymbol{\sigma}^2=(\mathbf{Z}\text{-}1\boldsymbol{\mu})^{\mathrm{T}}\Psi^{-1}(\mathbf{Z}\text{-}1\boldsymbol{\mu})^T n^{-1}$. The physics-based RM can be obtained by calculating the likelihood function of the original dataset (**X**, Φ) augmented with the new interpolating point ($\mathbf{X}^{\text{new}}$, Φ^{new}).

$$\Phi^{new}(\mathbf{X}^{new}) = \mu + r^T \psi^{-1}(\Phi - 1\mu) \tag{25}$$

where r is the $n\times1$ vector of correlations $\Psi(\mathbf{X}^{\text{new}}, \mathbf{X}_{l1})$ between the point ($\mathbf{X}^{\text{new}}$) to be predicted and the sample design points. By substituting Φ^{new} into Eq. (20), the state $\mathbf{Z}^{\text{new}}$ can be obtained at all nodes of the mesh system corresponding to any given input $\mathbf{X}^{\text{new}}$.

4.3.2 Level 2: Data-driven RM

High dimensional model representation

HDMR is a quantitative assessment and analysis tool for improving the efficiency of deducing high dimensional input-output behaviour of the system. HDMR can take into account the inherent uncertainty on input parameters and also presents the potential non-linearities and contributions due to the interactions between input parameters. HDMR expresses the model output $y \in \mathbf{Y}$ as a finite hierarchical cooperative function expansion in terms of its input variable $x \in \mathbf{X}$, as given by:

$$y = f_0 + \sum_{i=1}^{NH} f_i(x_i) + \sum_{i=1}^{NH}\sum_{j=i+1}^{NH} f_{ij}(x_i, x_j) + \cdots + f_{12\cdots NH}(x_1, x_2, \cdots, x_{NH}) \tag{26}$$

where NH is the size of input parameters, i and j index any two input parameters, and f_0=E[$f(x)$].

For most practical applications, the functions $f(x)$ containing more than two input parameters can often be ignored due to their fewer contributions compared to the former terms. Therefore, Eq. (26) can be simplified to a finite number of terms to calculate the predictor for any input variables. The data-driven RM can be obtained by:

$$\begin{aligned} &y = C + \sum_{i=1}^{NH}\sum_{kh=1}^{KH} A_{i,kh} \times x_i^{kh} + \sum_{i=1}^{NH}\sum_{j=i+1}^{NH}\sum_{kh=1}^{KH}\sum_{nh=1}^{KH} B_{i,j,kh,nh} \times x_i^{kh} \times x_j^{nh} \\ &i, j \in \{1, 2, 3, \cdots, NH\}, \qquad kh, nh \in \{1, 2, 3, \cdots, KH\} \end{aligned} \tag{27}$$

where C is a constant term, $A_{i,kh}$ and $B_{i,j,kh,nh}$ are the first and second-order coefficients, KH is the highest degree of the input variables. They can be regressed by using a specialized linear programming model, which is used to minimize the cumulative relative errors $\sum_m^M |y_m - \tilde{y}_m|$, $m \in$ {1,2,…,M}

between the outputs of RM (y_m) and CFD simulation ($\tilde{y}_m$), where M is the number of fitting datasets.

4.4 Model evaluation

In this work, the performance of the previously constructed models is thoroughly evaluated by both the training and generation errors (in terms of the average relative error, avgRE) between the outputs of bi-level RMs and the Fluent model. Herein, the training error is used to evaluate the reconstruction behaviour of the RMs at the design points, while the generalization error is to assess the prediction capability at unknown (interpolated) points that are not included in the sample set. Note that the generalization performance that truly reflects the prediction ability is of significant importance for the application of developed models, which are validated by using the cross-validation (CV) method. The latter randomly divides the observations into two mutually exclusive subsets. The training subset is used to construct the model, while the test subset unseen by the model during training is used to compute a prediction error. The original sample is repeatedly cut into a test subset and a training subset to assess and to obtain the reliable average error terms for the prediction of the left-out points. The optimal solution can be considered as a good approximation of the original distribution.

$$avgRE_t = \frac{1}{TE}\sum_{t=1}^{TE} RE_t = \frac{1}{TE}\sum_{t=1}^{TE} \frac{\left|O_t^{RM}(X^{test}) - O_t^{CFD}(X^{test})\right|}{O_t^{CFD}(X^{test})}, \forall O \in \{Y, Z\}, \forall t \in \{1, ..., TE\} \quad (28)$$

where TE is the number of training sets.

5. Multi-scale Optimization Model Formulation

The developed bi-level RMs of CWCTs, together with the shortcut models of other process units are further embedded in the multi-scale models of the cooling water network superstructure. As depicted in **Fig. 4**, the superstructure basically includes a set of circulating water streams with known inlet temperature and flow rates, which have the potential to be split into multiple sub-streams for

recycling or reuse. A set of CWCTs are in a parallel arrangement and each CWCT has the same cooling capacity and feeding flow rate. To cope with the variability of environmental parameters, each CWCT is equipped with a set of circulating pumps, intake fans, and spray pumps for flexibly adjustment of the flow rates of circulating water, air, and spray water, respectively. The cooled sub-streams of circulating water are merged into one and then mixed with make-up water and recycled circulating water. Finally, the circulating water streams at a satisfying temperature, exchange heat with process streams through the heat exchangers. In order to improve the model formulation, the developed data-driven RM of CWCTs is integrated with the overall process model of the system. A two-stage stochastic optimization problem is used to minimize the expected total annual cost $E(TAC)$ of the system, as given by:

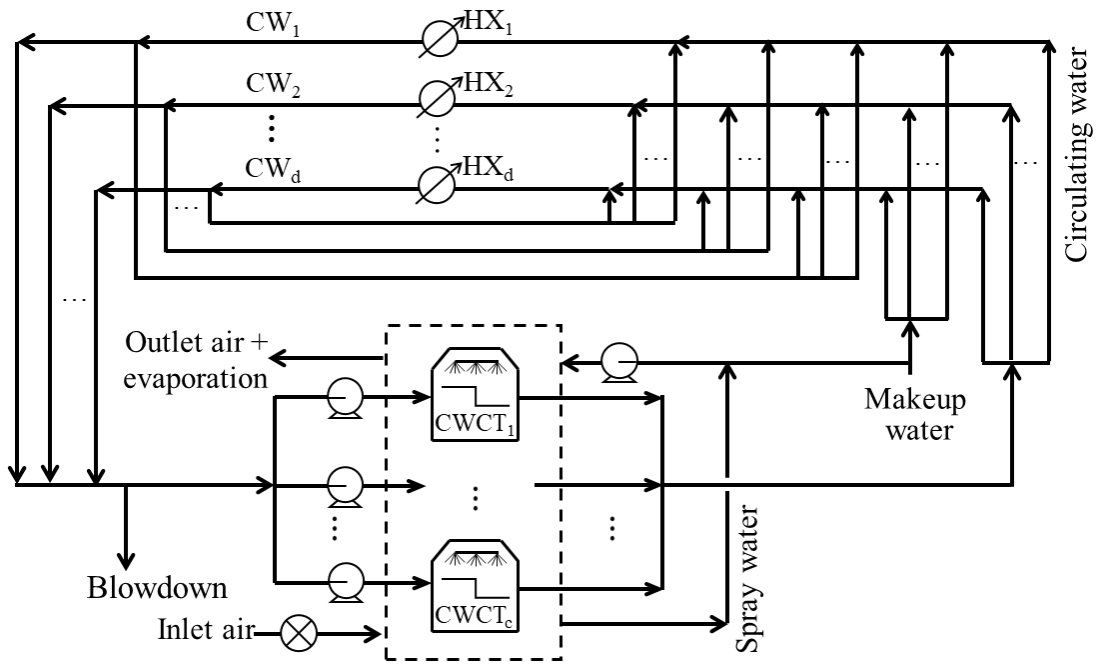

Fig. 4. Superstructure representation of a typical cooling water system.

$$
\begin{aligned}
Min \quad & E(TAC) = TC^{1st}(\mathbf{X}^{(1)}, \mathbf{X}^{(3),1st}, \mathbf{IX}) + \sum_{s=1}^{4}\sum_{n=1}^{N} Pro_{s,n} TC_{s,n}^{2nd}\left[\mathbf{X}^{(1)}, \mathbf{IX}, \mathbf{X}_{s,n}^{(2),2nd}, \mathbf{Y}_{s,n}(\mathbf{X}^{(1)}, \mathbf{X}_{s,n}^{(2),2nd})\right] \\
s.t. \quad & Eq^{1st}(\mathbf{X}^{(1)}, \mathbf{X}^{(3),1st}, \mathbf{IX}) = 0 \\
& IEq^{1st}(\mathbf{X}^{(1)}, \mathbf{X}^{(3),1st}, \mathbf{IX}) \le 0 \\
& \mathbf{X}^{(1),lb} \le \mathbf{X}^{(1)} \le \mathbf{X}^{(1),ub} \\
& \mathbf{X}^{(3),1st,lb} \le \mathbf{X}^{(3),1st} \le \mathbf{X}^{(3),1st,ub} \\
& \mathbf{IX}^{lb} \le \mathbf{IX} \le \mathbf{IX}^{ub} \\
& Eq_{s,n}^{2nd}\left[\mathbf{X}^{(1)}, \mathbf{IX}, \mathbf{X}_{s,n}^{(2),2nd}, \mathbf{Y}_{s,n}(\mathbf{X}^{(1)}, \mathbf{X}_{s,n}^{(2),2nd})\right] = 0, \ \ \forall s \in \{1,...,4\}, \forall n \in N^{2nd} \\
& IEq_{s,n}^{2nd}\left[\mathbf{X}^{(1)}, \mathbf{IX}, \mathbf{X}_{s,n}^{(2),2nd}, \mathbf{Y}_{s,n}(\mathbf{X}^{(1)}, \mathbf{X}_{s,n}^{(2),2nd})\right] \le 0, \ \ \forall s \in \{1,...,4\}, \forall n \in N^{2nd} \\
& \mathbf{Y}^{lb} \le \mathbf{Y}_{s,n}(\mathbf{X}^{(1)}, \mathbf{X}_{s,n}^{(2),2nd}) \le \mathbf{Y}^{ub}, \ \ \forall s \in \{1,...,4\}, \forall n \in N^{2nd}
\end{aligned}
\tag{29}
$$

where TC^{1st} and TC^{2nd} are part of the objective function, the former only depends on design variables (e.g. a function of capital cost), while TC^{2nd} relies on both design and operating variables (e.g. a function related to water consumption). For a stochastic programming problem, the equipment capacities (e.g. CWCTs, pumps, and fans) should be the same for all samples and thus the capital cost belongs to the sample-independent variable which are determined in the first stage by design equality Eq^{1st} and inequality constraint IEq^{1st}. The operating expenses determined in the second stage are formulated by stochastic functions (operational equality Eq^{2nd} and inequality constraint IEq^{2nd} on the feasibility of the process) to capture the variability in uncertain space. $\mathbf{X}^{(1)}$ and $\mathbf{X}^{(2),2nd}$ represent the deterministic and uncertain variables to the function of RMs; **IX** represents the remaining variables, $\mathbf{Y}(\mathbf{X}^{(1)}, \mathbf{X}^{(2),2nd})$ represents the outputs of the RM as a function of inputs $\mathbf{X}^{(1)}$ and $\mathbf{X}^{(2),2nd}$; $\mathbf{X}^{(3),1st}$ represents the design variables; $\mathbf{X}^{(1),lb}/\mathbf{X}^{(1),ub}$, $\mathbf{X}^{(3),1st,lb}/\mathbf{X}^{(3),1st,ub}$, $\mathbf{IX}^{lb}/\mathbf{IX}^{ub}$, and $\mathbf{Y}^{lb}/\mathbf{Y}^{ub}$ are corresponding lower/upper bounds of these variables; $Pro_{s,n}$ is the probability related to the occurrence of a specific sample n in season s, N^{2nd} is the set of samples. The model formulations are detailed in Supporting Information (SI).

6. Illustrative Example

Here, a small-size circulating water system is illustrated to introduce the detailed construction of

the bi-level RMs and the multi-scale optimization model to demonstrate the applicability of the proposed approach. The CFD simulation and stochastic programming problem associated with the multi-scale models are implemented via Fluent 16.0 and GAMS 24.7.1 modelling environment, respectively. Both models are solved on a workstation with Intel four processors Xeon e5 CPU @2.5 GHz and 32 GB RAM. In CFD modelling, the iterative default under-relaxation factors of 0.3 and 0.6 are used for pressure and momentum, respectively. In addition, the normalized residuals used for checking convergence are less than 10^{-3} for the momentum equations and less than 10^{-6} for the energy equations. For the two-stage stochastic optimization problem, it takes 10-90 min to obtain a feasible solution with a DICOPT[49] solver and the optimality gap of 10^{-9} at each iteration.

Formulation and evaluation of bi-level RMs

In this work, it is assumed the plant is located in Jieyang City, Guangdong province in the southern part of China. The original statistics of uncertain environmental parameters during the years 2015-2017 are retrieved from the government database (http://www.noaa.gov), as provided in **Table S1** of the SI. All seasons within the chosen years are taken into account. With an initial sample size of 50, the optimal number of samples generated by HSS is 300 for spring, 200 for summer, 200 for autumn, and 200 for winter (see **Table S2** in SI). **Fig. 5** depicts the PDFs of dry-bulb temperature and relative humidity for the four seasons, along with their mean value and standard derivation. As shown, it is apparent that both uncertain variables have remarkably different statistical moments among the seasons and range over a large span throughout the year.

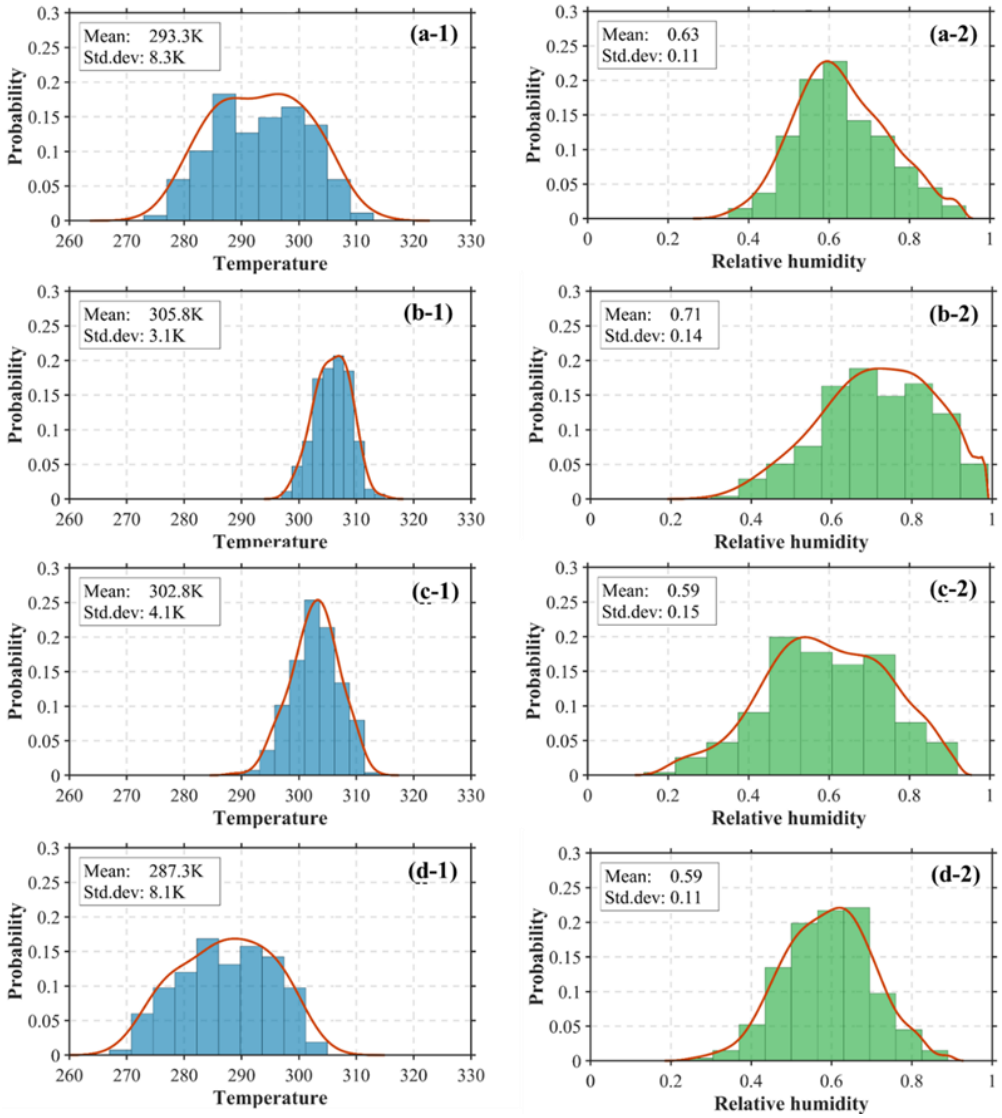

Fig. 5. PDFs of dry-bulb temperature and relative humidity.(a)spring;(b)summer;(c)autumn;(d)winter

The results of the reconstruction behaviour of the developed physics-based RM at the design points of the CWCT are presented in **Table 2**. Here, we systemically compare the avgRE of four monitored states with respect to the temperature, pressure, velocity, and H_2O mass fraction between the outputs of physics-based RM and Fluent model in four seasons. The statistical values of avgRE are very similar, with a tiny range between 2.44×10^{-17}~5.73×10^{-17} for temperature, 3.81×10^{-12}~5.48×10^{-11} for pressure, 2.02×10^{-8}~5.39×10^{-7} for velocity, and 7.11×10^{-16}~1.84×10^{-14} for H_2O mass fraction. Comparing these results, it may be concluded that the outputs of physics-based RM maintain high accuracy and no observable difference at the design points for all cases.

Table 2. Results of avgRE for the physics-based RM

Season	Temperature	Pressure	Velocity	H_2O mass fraction
Spring	3.18×10^{-17}	5.48×10^{-11}	2.03×10^{-8}	1.84×10^{-14}
Summer	2.44×10^{-17}	2.70×10^{-11}	7.88×10^{-8}	7.11×10^{-16}
Autumn	2.89×10^{-17}	1.43×10^{-11}	5.39×10^{-7}	2.98×10^{-15}
Winter	5.73×10^{-17}	3.81×10^{-12}	2.02×10^{-8}	1.83×10^{-14}

The reconstruction behaviour of the physics-based RM is further assessed at unknown points. Four typical cases that correspond to the mean values of the input variables in each season are shown in **Fig. 6~9**. For each case, four monitored field profiles of state variables (temperature, pressure, velocity, and H_2O mass fraction) inside the tower are used to visually represent the reconstruction behaviour of physics-based RM. It can be seen from these figures that the contours of the field profiles predicted using physics-based RM are comparable to those from Fluent model and the distortions of the contours in some figures (i.e. velocity profiles) are even hard to observe. Herein, it is worth noting that the developed RMs are capable of sharply reducing the computational time and resources as compared to the Fluent model. For example, completing a Fluent model requires approximately three days for an investigated case, while the developed RMs take less than 2 seconds.

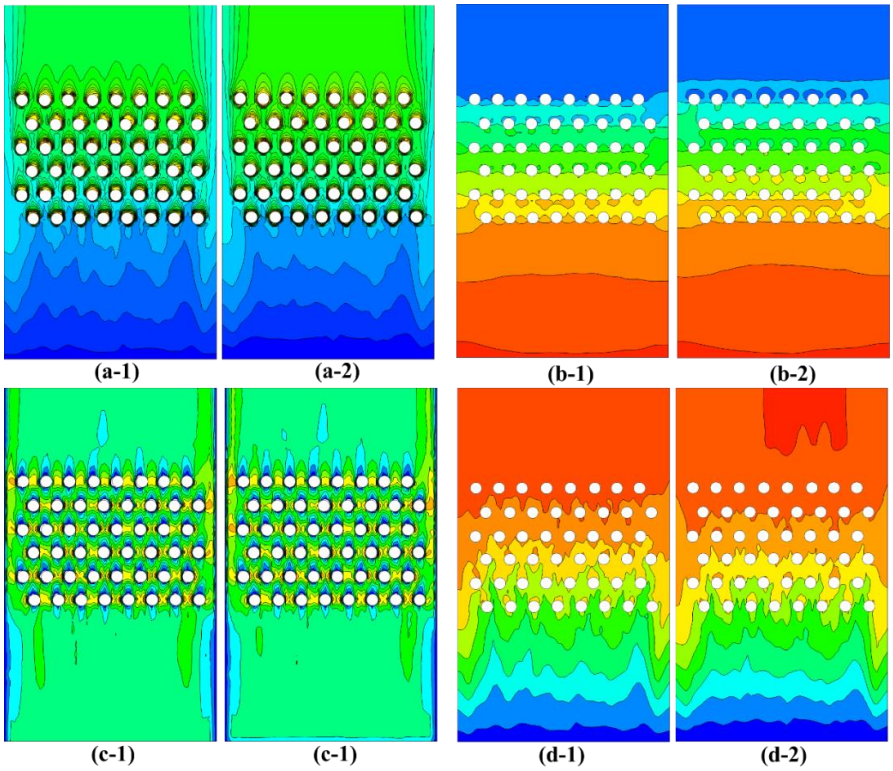

Fig. 6. Contour lines of (a) temperature, (b) pressure (c) velocity, and (d) H_2O mass fraction in the case of Spring predicted by Fluent model (left) and physics-based RM (right).

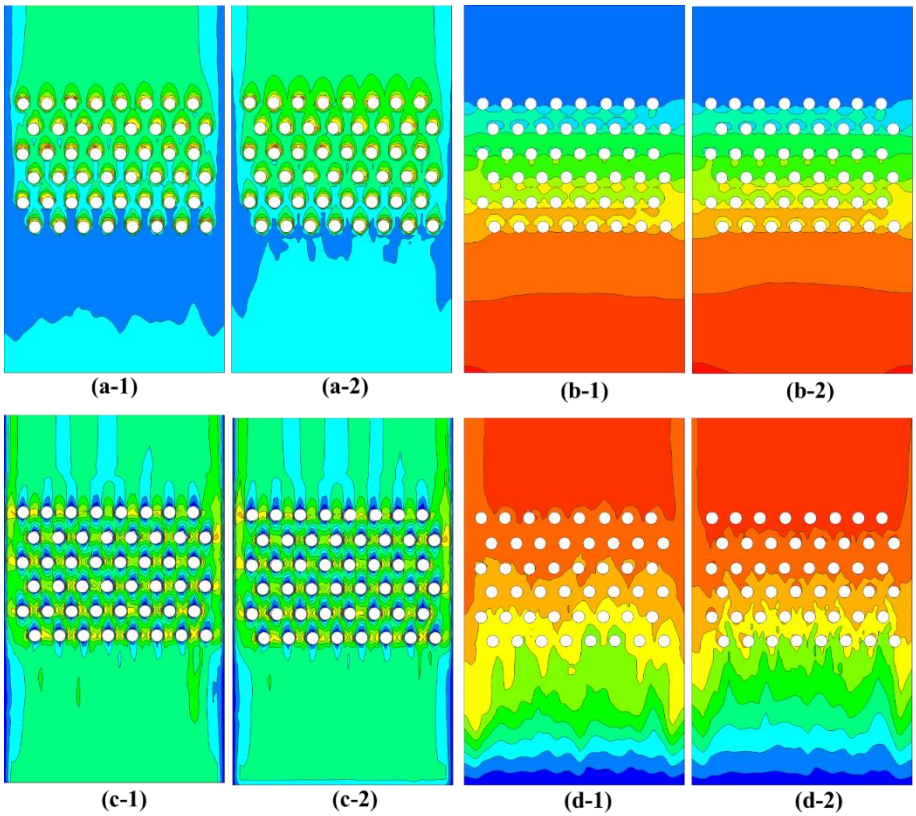

Fig. 7. Contour lines of (a) temperature, (b) pressure (c) velocity, and (d) H_2O mass fraction in the case of Summer predicted by Fluent model (left) and physics-based RM (right).

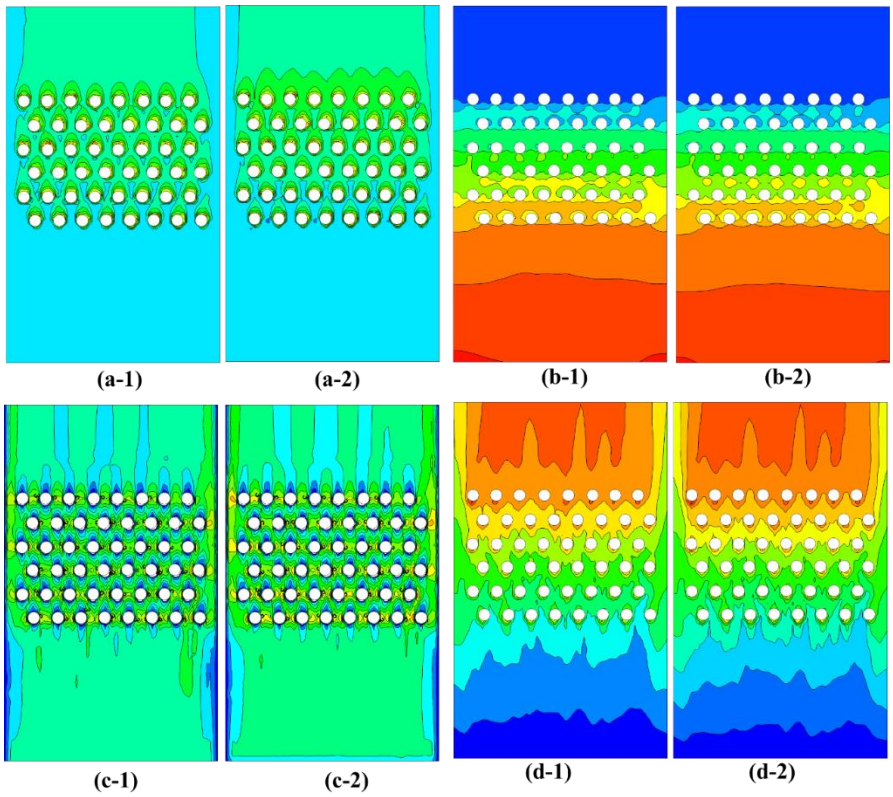

Fig. 8. Contour lines of (a) temperature, (b) pressure (c) velocity, and (d) H_2O mass fraction in the case of Autumn predicted by Fluent model (left) and physics-based RM (right).

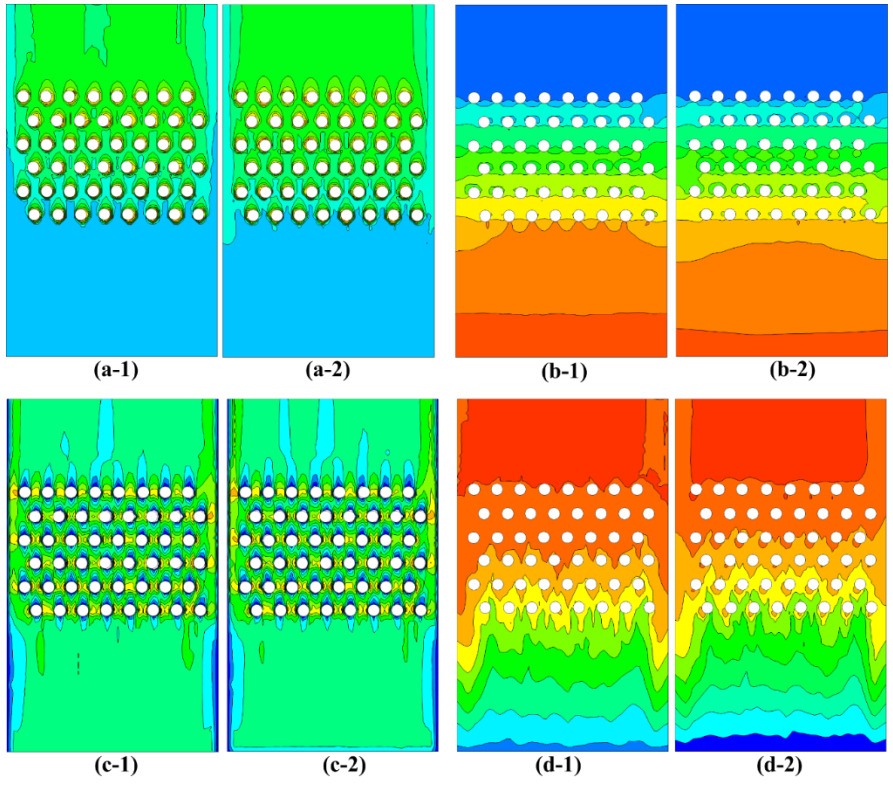

Fig. 9. Contour lines of (a) temperature, (b) pressure (c) velocity, and (d) H_2O mass fraction in the case of Winter predicted by Fluent model (left) and physics-based RM (right).

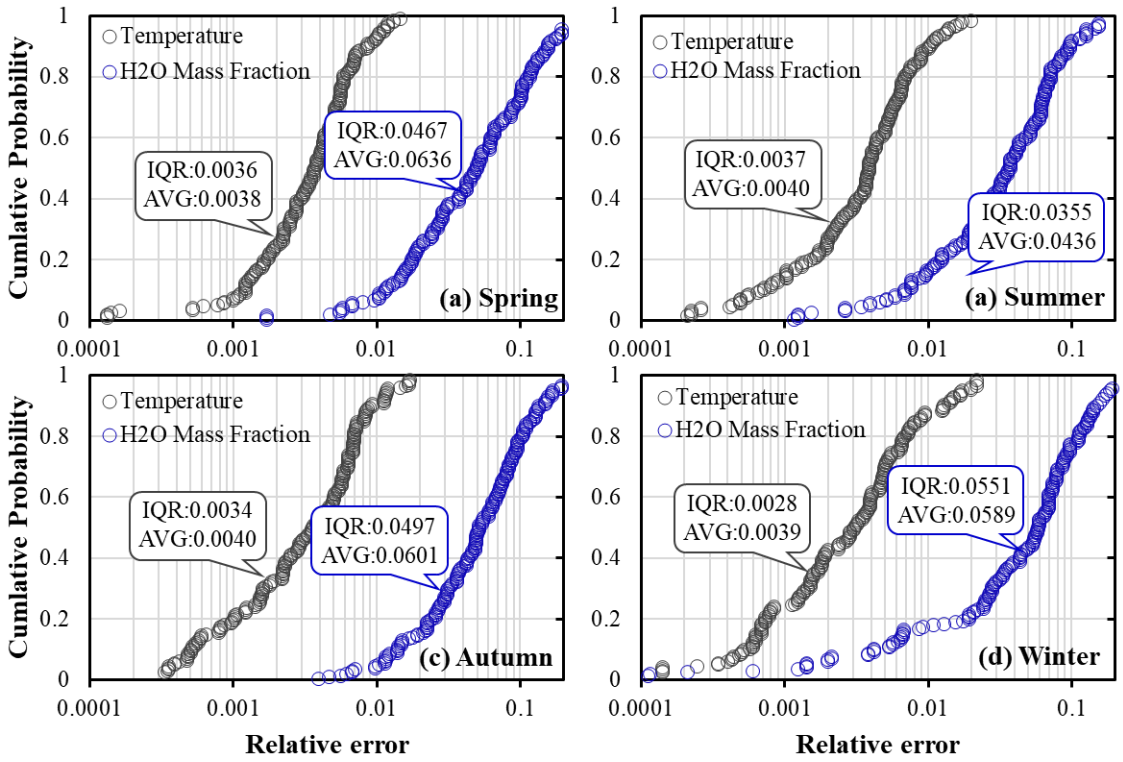

Fig. 10. Relative errors between data-driven RM and Fluent results. (a) spring; (b) summer; (c) autumn; and (d) winter.

Fig. shows the relative errors of temperature and H_2O mass fraction by implementing the CV of the data-driven RM with Fluent results. As shown, the relative errors of outlet air temperature for all 900 samples are less than 0.02, while more than 70% of the relative errors of H_2O mass fraction are less than 0.1. In addition, both avgRE and interquartile range (IQR) of the relative errors are presented in **Fig.** . The former indicator ranges from 0.0038 to 0.0040 for outlet air temperature, and from 0.0436 to 0.0636 for H_2O mass fraction. The latter range from 0.0028 to 0.0037 for the outlet air temperature, and from 0.0355 to 0.0636 for H_2O mass fraction. Hence, it can be concluded that the developed data-driven RM for the CWCT offers reasonable and sufficient confidence for further use for integration within the cooling tower systems models for optimization.

Multi-scale optimization of the cooling water system

In the multi-scale optimization model, techno-economic evaluation is performed to consider plant

capital and operating costs, as well as equipment performance simultaneously, by integrating a cooling water network and CWCTs. To solve the stochastic optimization problem, stochastic samples for each season are first generated by setting an initial size of 50, with a 95% confidence interval. The optimal sizes of the samples were determined as 300 for spring, 100 for summer, 200 for autumn, and 200 for winter, and all the generated samples have passed the Chi-squared test (see **Table S3** in SI). The design and operating variables and the corresponding ranges used in the optimization problem are listed in **Table 1**, which are consistent with those used in building the data-driven RM. To simplify the optimization model stated in Eq. (29), the inner diameter of tubes installed in the CWCT is assumed to be a fixed value (d^{tube}=0.01m) and the cooling water system is assumed to consist of three circulating water streams, and their corresponding flow rates, inlet and target temperatures are listed in **Table 3**.

In this study, a deterministic optimization model is also developed to emphasize the importance of the stochastic approach. It should be highlighted that the deterministic model can be easily obtained from the proposed stochastic approach by considering a representative sample. This single sample corresponds to the mean value of uncertain environmental parameters for the whole year (297.3 K for the dry-bulb temperature, 63.0% for the relative humidity of inlet air). Next, the equipment capacities obtained from this single sample are fixed in the model and compare with the stochastic model to further assess the impact of uncertainty on the techno-economic performances of the CWCTs and the whole cooling water system.

Table 3. Basic data of circulating water streams

Stream	Flow rate (m^3/h)	Inlet temperature (K)	Target temperature (K)
CW_1	216	324	[293, 315]
CW_2	548	316	[293, 311]
CW_3	468	311	[293, 309]

The optimal solutions obtained from the deterministic and stochastic approaches dispatches the inlet circulating water streams for their appropriate sinks in the cooling water network. As shown in **Fig.** , it is notable that the stochastic and deterministic solutions have the same distributed network structure, which contains four units of CWCTs, circulating pumps, spray pumps, eight intake fans, and three heat exchangers. In this figure, the inlet circulating water streams denoted by the grey lines exchange heat with process streams via heat exchangers, and their flow rates stay constant as those listed in **Table 3**. The distributed loads of other streams in the cooling water network (i.e. split and recycled streams), as well as the operating conditions of the CWCTs (i.e. inlet air and spray water) are constantly changing with the variation of environmental parameters in each season.

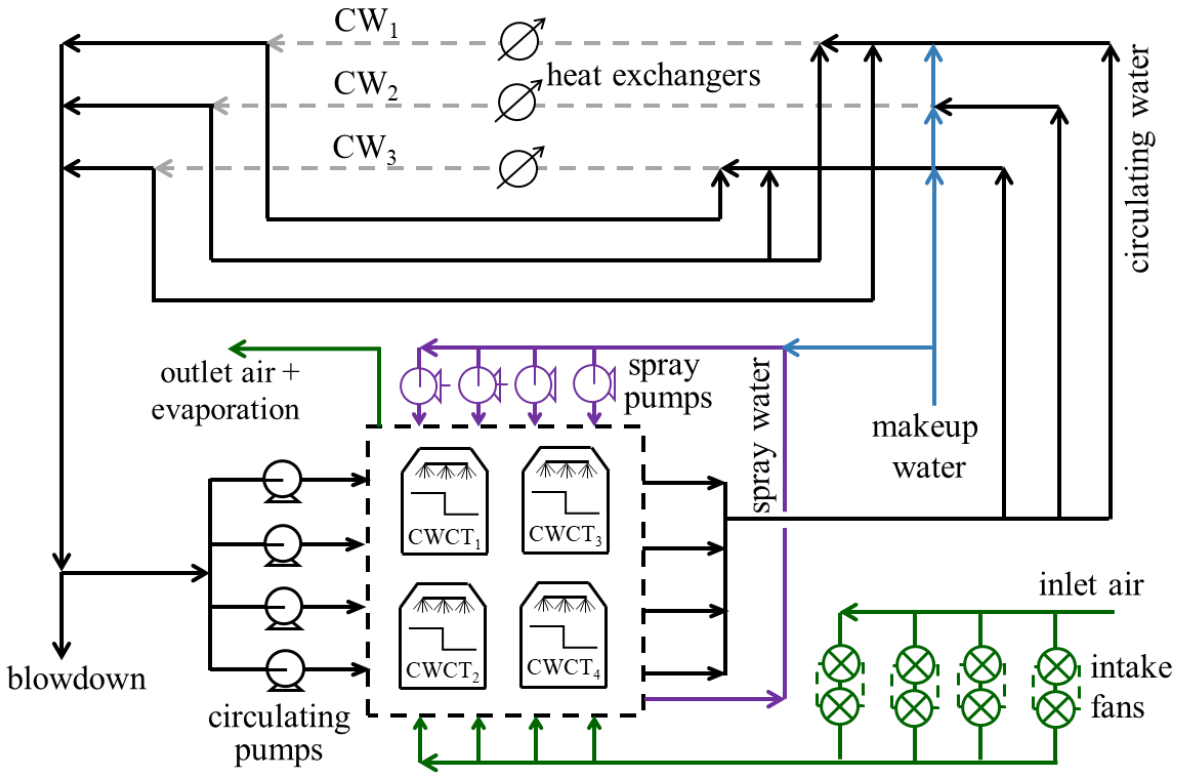

Fig. 11. The optimal cooling water network obtained from the stochastic and deterministic solutions.

Fig. a compares the breakdown of expected TAC of cooling water system for both deterministic and stochastic solutions. The annual capital cost based on the samples of one season is equal to that

based on the other one due to the constraints on the design variables for the same solution. However, note that the two optimal solutions lead to different annual capital costs, though they yield the same cooling water network shown in **Fig.** . This is mainly attributed to the various design capacities and geometry sizes of the installed CWCTs and other process equipment in the same cooling water network. For instance, in the case of the same inner diameter (d^{tube}=0.01 m), the optimal number of tube bundles assembled in each CWCT has grown from 407 for the deterministic solution to 519 for the stochastic solution. The corresponding design capacities of auxiliary equipment such as circulating pumps, spray pumps, and intake fan increase by 27.4%, 32.6%, and 29.4%, respectively. Thus, the annual capital cost increases from $\$3.76\times10^5$ for the deterministic solution to $\$4.04\times10^5$ for the stochastic solution, which accounts for 59.4% and 67.9% of the expected TAC, respectively.

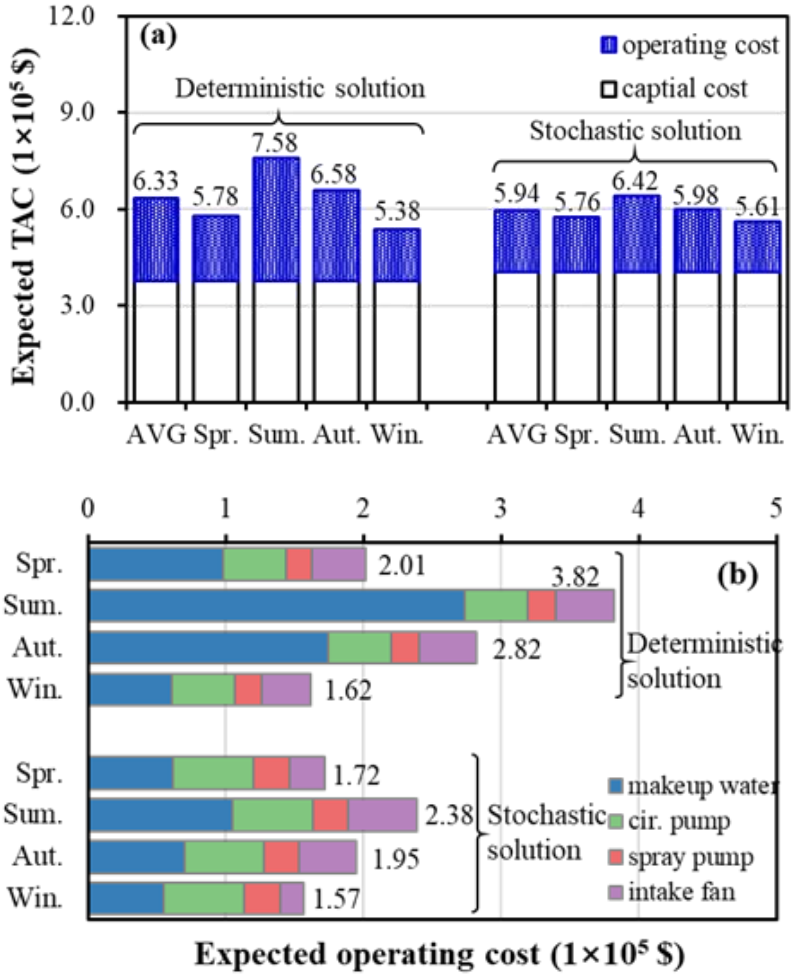

Fig. 12. The breakdowns of (a) expected TAC and (b) operating cost for four seasons.

Though the stochastic solution results in a greater annual capital cost, the expected TAC based on all 800 samples (detonated by AVG in **Fig. a**) obtained from this solution is $\$5.94\times10^5$, which is still lower than that of the deterministic one ($\$6.33\times10^5$). This reduction mainly stems from the significant reduction of operating cost, which is $\$2.57\times10^5$ for the deterministic solution and $\$1.91\times10^5$ for the stochastic solution. To be more specific, **Fig. b** shows that the mean value of operating expenses for utility usage cuts down from $\$2.01\times10^5$ to $\$1.72\times10^5$ for spring, $\$3.82\times10^5$ to $\$2.38\times10^5$ for summer, $\$2.82\times10^5$ to $\$1.95\times10^5$ for autumn, and $\$1.62\times10^5$ to $\$1.57\times10^5$ for winter. Among them, it is obvious that the hot seasons would lead to higher operating expenses mainly due to the significantly increased consumption of makeup water. Especially, in summer the operating expense of makeup water had a sharp increase from $\$1.05\times10^5$ for the stochastic solution to $\$2.74\times10^5$ for the deterministic solution, which accounts for 44.1% and 71.7% of the operating cost, respectively. From the results, it can be concluded that for the stochastic solution, the reduction in the capital cost achieved by decreasing the equipment capacities is less significant and not enough to make up the loss due to the increased operating costs of CWCTs. The stochastic solution allows for a certain design margin of CWCTs to reduce the impacts of the variability of environmental conditions and to avoid the abnormal running conditions in extreme scenarios. This highlights the importance of considering the uncertainty of environmental parameters in the robust design of the cooling water system.

Fig. 7 shows the varying inputs of inlet air, spray water, and makeup water that corresponds to CWCTs for all 800 samples. From **Fig. 7a**, it is seen that the velocity of inlet air for the stochastic solution is mostly lower than that of the deterministic one, especially in cold seasons like spring and winter. For example, the velocity of inlet air for the deterministic solution has mostly reached the upper

bound, 2.5 m/s, indicating the CWCT operates in a full-load state. The main reason is that the increased cooling capacity of CWCTs obtained from the stochastic solution has a greater quantity of tube bundles and larger heat exchanger areas, which reduce the required amount of inlet air as compared to the deterministic solution. However, a larger cooling capacity also means that more spray water is required to form the liquid film on the surface of the coil tubes. From **Fig. 7b**, it is seen that for all generated samples, the average usage amount of spray water has increased by about one-third, i.e. from 13.6 kg/s (deterministic solution) to 18.6 kg/s (stochastic solution). Besides, note that the makeup water consumption is equal to the sum of the blowdown and evaporation losses according to mass balance, and the blowdown contributes 60~80% of the total. Thus, though the increased usage of spray water leads to greater evaporation losses, the stochastic solution has remarkable advantages in reducing the amounts of circulating water load and blowdown by properly increasing the cooling capacity of CWCT. On the contrary, the CWCT within the constraints is almost operated at full load for the deterministic solution, particularly in summer, no matter how the operating variables (inlet air, spray water, and inlet stream) are manipulated. As shown in **Fig. 7c**, in order to meet the cooling target of circulating water, the amount of makeup water greatly reduces from 6.67~72.9 m^3/h (deterministic solution) to 6.67~49.5 m^3/h (stochastic solution).

It is challenging to assess the accuracy of the solution optimality and the underlying model in the presence of model reduction and assumptions. In this study, we randomly selected Sample 28 in the Spring case (dry-bulb temperature 285.5 K and relative humidity 57.7% of inlet air, see **Fig. 7a-1** and **Table S3** in **SI)** to validate the data-driven RM of the CWCT at the optimal solution. Are listed in **Table 4**, compared with the FLUENT results, the relative errors of temperature and H_2O mass fraction of the outlet air are only 0.0019 and 0.0287, respectively. The magnitudes of these relative errors fall

within the range of 0.0001~0.01 and 0.001~0.11, which are in line with the ranges shown in **Fig. 10a**. The error evaluation based on Sample 28 indicates that the RM-based optimization model achieves an optimal result that retains the optimality of the original high-fidelity model for the same input variables.

Table 4. Error evaluation for Sample 28 in the Spring case

Method	Temperature of outlet air (K)	Relative error	H_2O mass fraction of outlet air	Relative error
Data-driven RM	311.8	0.0019	0.0338	0.0287
FLUENT model	312.4		0.0348	

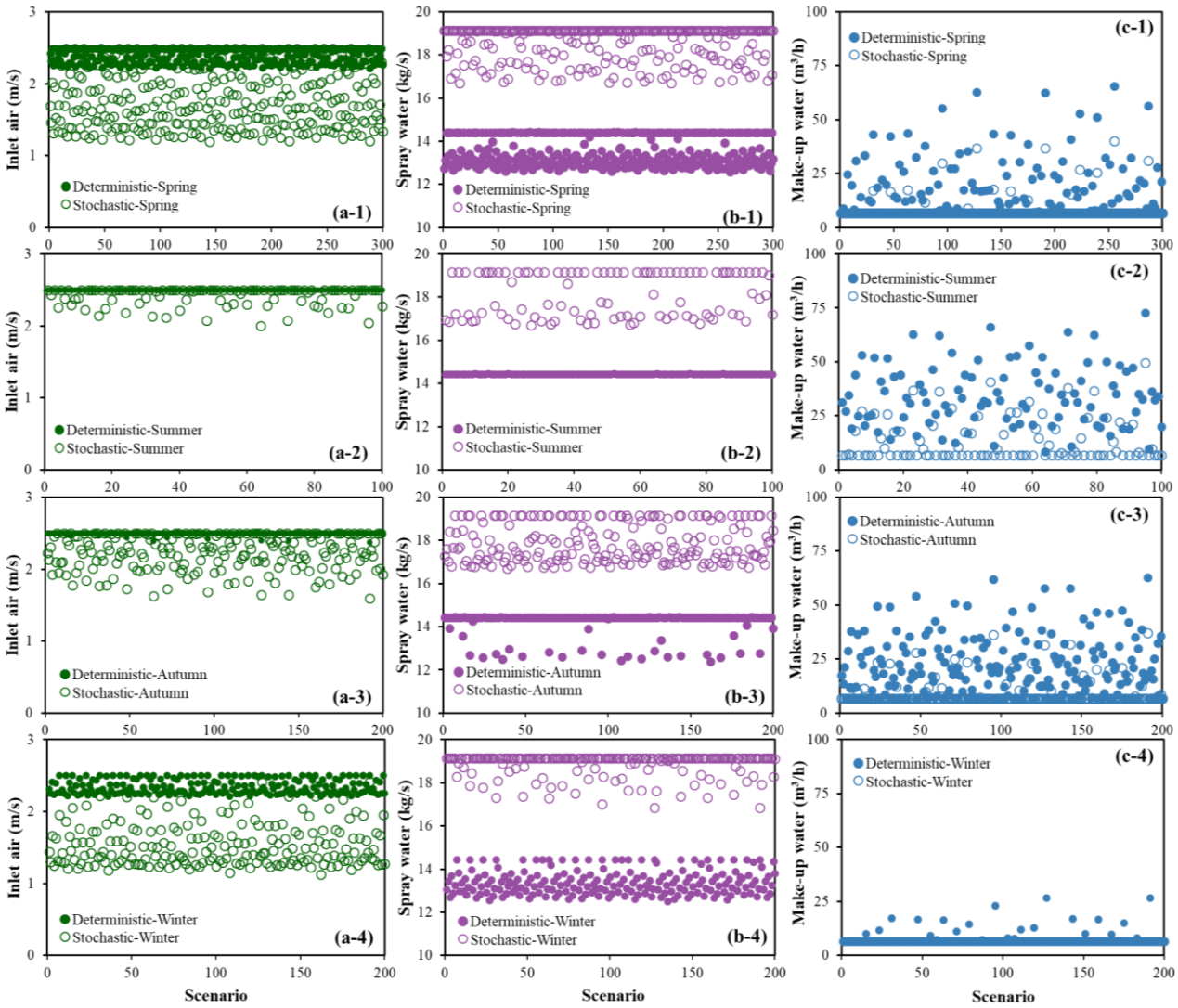

Fig. 7. The optimal values of key operating variables of the system obtained from the deterministic and stochastic solutions.

As aforementioned, the proposed multi-scale optimization approach can not only present the optimal values of objective and the corresponding operating and design variables for the whole system, but also reconstructs the high-fidelity fluid dynamics and reveals the complex thermal and flow behaviours via physics-based RM. For better understanding of the influence of optimal solutions on heat-mass transfer processes inside CWCTs, we still selected sample 28 in spring for better physical inspection of field profiles. For this selected sample, **Fig. 8** indicates that as the inlet air flows upwards and contacts with falling spray water, it is gradually saturated with water vapour and the longitudinal temperature gradient appears more evident between the coil tubes. It is interesting that the two optimal solutions yield almost the same temperature profiles as air flow. The amplification of the selected temperature field further indicates that they have the same maximum and minimum contour lines of temperature, which are 313K and 305 K at the top and bottom of the tubes, respectively. This consistency in temperature profile is mainly due to the fact that the overall heat transfer process is mainly controlled by the maximum heat transfer potential of saturated moist air under the same operating temperature of inlet air, spray water, and circulating water.

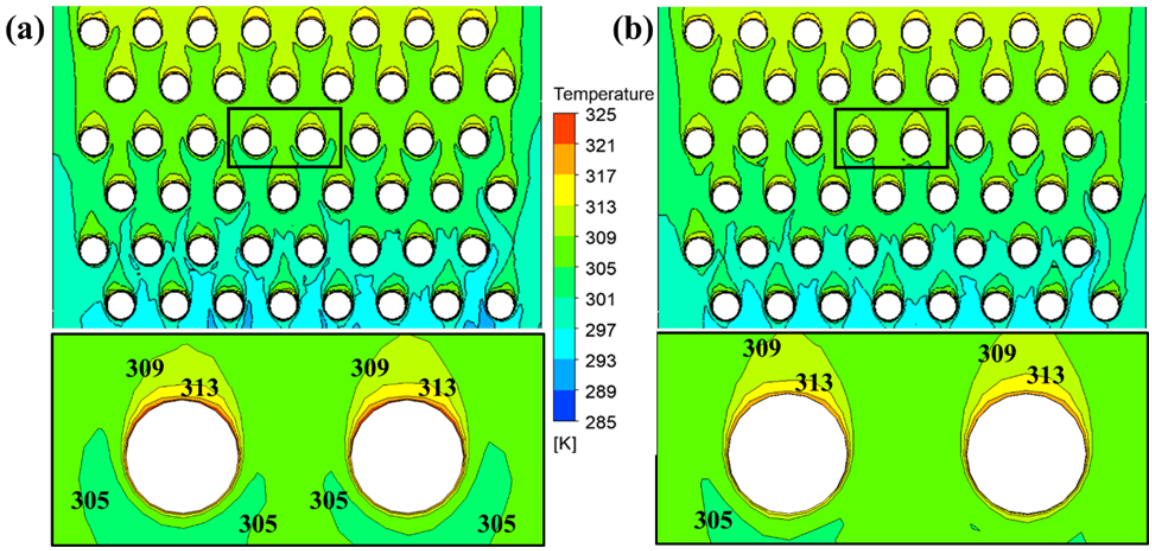

Fig. 8. Contours of fluid temperature inside CWCTs obtained from (a) deterministic model and (b) stochastic model.

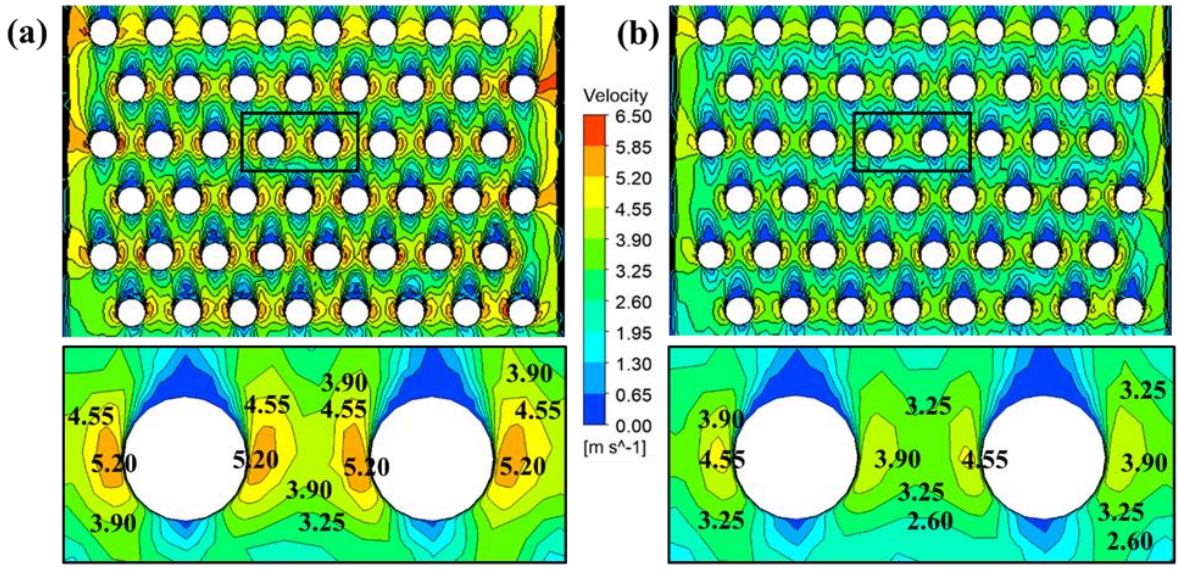

Fig. 9. Contours of inlet air velocity inside CWCTs obtained from (a) deterministic model and (b) stochastic model.

As the inlet air flows upwards and encounters the coil tubes at the stagnation points, most of its kinetic energy is converted into pressure energy according to the Bernoulli equation. Thus, the pressure profile is closely related to the velocity profile inside a cooling tower. As shown in **Fig. 9** Fig. **10**, the contours of inlet air velocity are significantly reduced, while the contours of fluid pressure increase accordingly in the surrounding region of the stagnation points. As the inlet air continues to flow upwards, the pressure gradient along the flow direction of inlet air becomes negative due to the gradual shrinkage of the flow path, making the air flow at the boundary layer to be in an accelerated speed state. The maximum value of the contours of inlet air velocity can be found at the left and right ends of each tube. Thereafter, under the combined effects of the shear stress and pressure gradient, the contours of velocity at the boundary layer decrease rapidly and reach their lowest value at the upper-point of the tubes.

In **Fig. 10**, it is seen from the amplification of the selected field that the pressure contour lines have about one-third growth from 27.2~36.0 Pa for the stochastic solution to 18.4~27.2 Pa for the

deterministic solution. Similarly, it is seen from **Fig. 10** that the velocity contour lines of the inlet air at the same location increased from 3.90~4.55 m/s for the stochastic solution to 3.25~5.20 m/s for the deterministic solution. It should be noted that in practice the increased profiles of air velocity and fluid pressure have an adverse effect on the long-term operation of cooling towers. Also, note that the selected Sample 28 corresponds to normal weather conditions over the whole year. As the CWCTs operates at more extreme weather conditions, such as in summer, the cooling capacity of CWCTs would be significantly weakened mainly due to the increased temperature and relative humidity of the inlet air. For the deterministic solution, it is insufficient to cool down the inlet circulating water by only manipulating the variables of CWCT within the specified variable space, unless the consumption of makeup water is increased substantially. Instead, the stochastic solution is capable of reducing the operational and economic risks of the whole cooling water system through fully accommodating the uncertainty of environmental parameters and flexibly increasing the capacity of equipment.

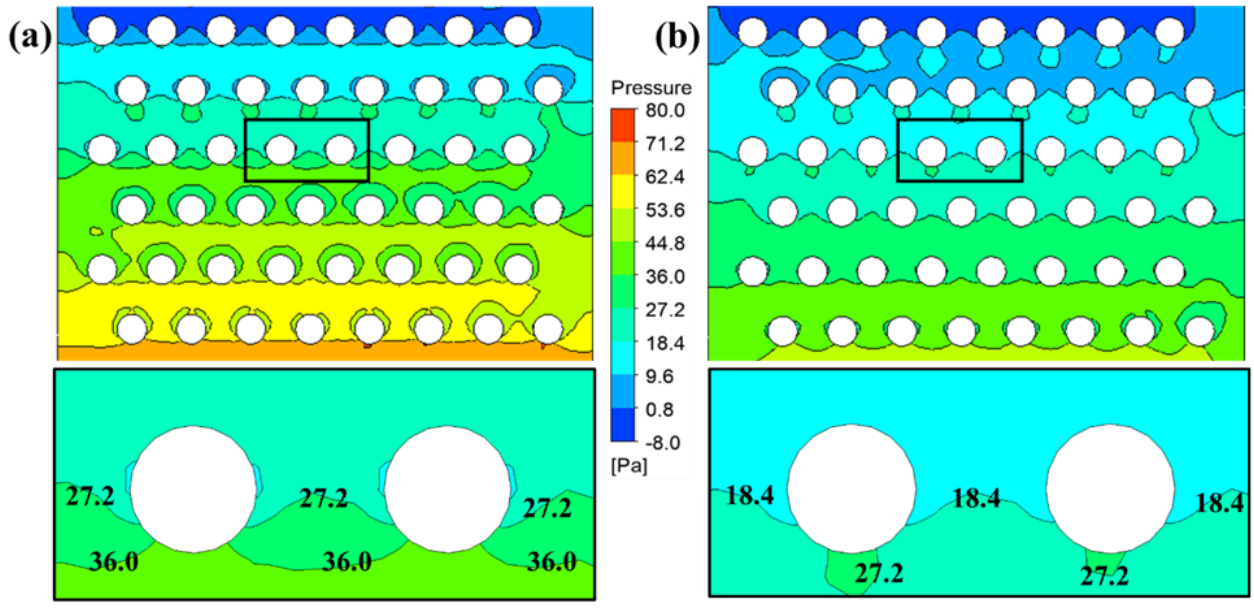

Fig. 10. Contours of fluid pressure inside CWCTs obtained from (a) deterministic model and (b) stochastic model.

7. Conclusion

In this study, a tailored framework based on model reduction was proposed for multi-scale stochastic optimization of the cooling water system with counter-current CWCTs under the uncertainty on environmental parameters. The model reduction methodology used for processing the input data and generating bi-level RMs for CWCTs included four statistical steps: optimal DoE, multi-sample CFD simulation, reduced model construction, and model evaluation. In particular, based on rigorous CFD simulation, a fast data-driven and physics-based RMs was constructed by utilizing HDMR and combined PCA-Kriging interpolation, respectively, to closely approximate the high-fidelity CWCTs models. The developed bi-level RMs were embedded in a multi-scale optimization model for performing integrated design and management of the CWCTs and cooling water system. This optimization model employed sampling-based stochastic programming and the heterogeneous integration of unit-specific shortcut models and detailed models of CWCTs.

A small-scale industrial example was presented to illustrate the effectiveness and benefits of the proposed approach by comparing with a deterministic approach. The optimization results showed that the developed bi-level RMs provided a good approximation of CWCTs and resulted in a significant reduction in CPU time. Besides, the stochastic solution can reduce makeup consumption and save costs as compared with the deterministic solution, though it properly increases the capital costs of CWCTs and other auxiliary equipment. More importantly, the stochastic solution can effectively reduce the impact of the variability of weather conditions and avoid the abnormal running of the cooling water systems in extreme scenarios. The corresponding field visualization of CWCTs through the physics-based RM further reflected the importance of consideration of the stochastic approach and uncertainty in the robust design of cooling water systems.

Acknowledgments

Financial supports from the National Natural Science Foundation of China (No. 51776228, 21606261), the Science and Technology Planning Project of Guangdong Province (No. 2016B020243002) are gratefully acknowledged.

References

1. Gan, G.; Riffat, S. B., Numerical simulation of closed wet cooling towers for chilled ceiling systems. *Appl Therm Eng* **1999,** 19, (12), 1279-1296.

2. Xie, X. C.; He, C.; Xu, T.; Zhang, B. J.; Pan, M.; Chen, Q. L., Deciphering the thermal and hydraulic performances of closed wet cooling towers with plain, oval and longitudinal fin tubes. *Appl Therm Eng* **2017,** 120, 203-218.

3. Hasan, A.; Siren, K., Theoretical and computational analysis of closed wet cooling towers and its applications in cooling of buildings. *Energ Buildings* **2002,** 34, (5), 477-486.

4. Facao, J.; Oliveira, A. C., Thermal behaviour of closed wet cooling towers for use with chilled ceilings. *Appl Therm Eng* **2000,** 20, (13), 1225-1234.

5. Stabat, P.; Marchio, D., Simplified model for indirect-contact evaporative cooling-tower behaviour. *Appl Energ* **2004,** 78, (4), 433-451.

6. Xia, Z. Z.; Chen, C. J.; Wang, R. Z., Numerical simulation of a closed wet cooling tower with novel design. *Int J Heat Mass Tran* **2011,** 54, (11-12), 2367-2374.

7. Papaefthimiou, V. D.; Rogdakis, E. D.; Koronaki, I. P.; Zannis, T. C., Thermodynamic study of the effects of ambient air conditions on the thermal performance characteristics of a closed wet cooling tower. *Appl Therm Eng* **2012,** 33-34, 199-207.

8. Zheng, W. Y.; Zhu, D. S.; Zhou, G. Y.; Wu, J. F.; Shi, Y. Y., Thermal performance analysis of closed wet cooling towers under both unsaturated and supersaturated conditions. *Int J Heat Mass Tran* **2012,** 55, (25-26), 7803-7811.

9. Zhu, D. S.; Zheng, W. Y.; Zhou, G. Y.; Wu, J. F.; Shi, Y. Y., Computational Analysis of Closed Wet Cooling Towers. *Numer Heat Tr a-Appl* **2013,** 63, (5), 396-409.

10. Xie, X.; Liu, H.; He, C.; Zhang, B.; Chen, Q.; Pan, M., Deciphering the heat and mass transfer behaviors of staggered tube bundles in a closed wet cooling tower using a 3-D VOF model. *Appl Therm Eng* **2019,** 161, 114202.

11. Lang, Y. D.; Malacina, A.; Biegler, L. T.; Munteanu, S.; Madsen, J. I.; Zitney, S. E., Reduced Order Model Based on Principal Component Analysis for Process Simulation and Optimization. *Energ Fuel* **2009,** 23, (3-4), 1695-1706.

12. Yu, M. Z.; Miller, D. C.; Biegler, L. T., Dynamic Reduced Order Models for Simulating Bubbling

Fluidized Bed Adsorbers. *Ind Eng Chem Res* **2015,** 54, (27), 6959-6974.

13. Park, K.; Oh, P. K.; Lim, H. J., The application of the CFD and Kriging method to an optimization of heat sink. *Int J Heat Mass Tran* **2006,** 49, (19-20), 3439-3447.

14. Bodjona, S.; Girault, M.; Videcoq, E.; Bertin, Y., Reduced order model of a two-phase loop thermosyphon by modal identification method. *Int J Heat Mass Tran* **2018,** 123, 637-654.

15. Hasan, M. M. F.; Baliban, R. C.; Elia, J. A.; Floudas, C. A., Modeling, Simulation, and Optimization of Postcombustion CO2 Capture for Variable Feed Concentration and Flow Rate. 1. Chemical Absorption and Membrane Processes. *Ind Eng Chem Res* **2012,** 51, (48), 15642-15664.

16. Boukouvala, F.; Gao, Y. J.; Muzzio, F.; Ierapetritou, M. G., Reduced-order discrete element method modeling. *Chem Eng Sci* **2013,** 95, 12-26.

17. Barrasso, D.; Tamrakar, A.; Ramachandran, R., A reduced order PBM-ANN model of a multi-scale PBM-DEM description of a wet granulation process. *Chem Eng Sci* **2014,** 119, 319-329.

18. Rogers, A.; Ierapetritou, M. G., Discrete Element Reduced-Order Modeling of Dynamic Particulate Systems. *Aiche J* **2014,** 60, (9), 3184-3194.

19. Quirante, N.; Javaloyes, J.; Caballero, J. A., Rigorous design of distillation columns using surrogate models based on Kriging interpolation. *Aiche J* **2015,** 61, (7), 2169-2187.

20. Narasingam, A.; Kwon, J. S.-I., Development of local dynamic mode decomposition with control: Application to model predictive control of hydraulic fracturing. *Comput Chem Eng* **2017,** 106, 501-511.

21. Sidhu, H. S.; Narasingam, A.; Siddhamshetty, P.; Kwon, J. S.-I., Model order reduction of nonlinear parabolic PDE systems with moving boundaries using sparse proper orthogonal decomposition: Application to hydraulic fracturing. *Comput Chem Eng* **2018,** 112, 92-100.

22. Narasingam, A.; Siddhamshetty, P.; Sang-Il Kwon, J., Temporal clustering for order reduction of nonlinear parabolic PDE systems with time-dependent spatial domains: Application to a hydraulic fracturing process. *Aiche J* **2017,** 63, (9), 3818-3831.

23. Rowley, C. W.; MeziĆ, I.; Bagheri, S.; Schlatter, P.; Henningson, D. S., Spectral analysis of nonlinear flows. *J Fluid Mech* **2009,** 641, 115-127.

24. Palmer, K.; Realff, M., Optimization and Validation of Steady-State Flowsheet Simulation Metamodels. *Chemical Engineering Research and Design* **2002,** 80, (7), 773-782.

25. Palmer, K.; Realff, M., Metamodeling Approach to Optimization of Steady-State Flowsheet

Simulations: Model Generation. *Chemical Engineering Research and Design* **2002,** 80, (7), 760-772.

26. Fernandes, F. A. N., Optimization of Fischer-Tropsch synthesis using neural networks. *Chem Eng Technol* **2006,** 29, (4), 449-453.

27. Lang, Y. D.; Zitney, S. E.; Biegler, L. T., Optimization of IGCC processes with reduced order CFD models. *Comput Chem Eng* **2011,** 35, (9), 1705-1717.

28. Hasan, M. M. F.; Baliban, R. C.; Elia, J. A.; Floudas, C. A., Modeling, Simulation, and Optimization of Postcombustion CO2 Capture for Variable Feed Concentration and Flow Rate. 2. Pressure Swing Adsorption and Vacuum Swing Adsorption Processes. *Ind Eng Chem Res* **2012,** 51, (48), 15665-15682.

29. Quirante, N.; Javaloyes-Anton, J.; Caballero, J. A., Hybrid simulation-equation based synthesis of chemical processes. *Chem Eng Res Des* **2018,** 132, 766-784.

30. Ye, W. H.; You, F. Q., A computationally efficient simulation-based optimization method with region-wise surrogate modeling for stochastic inventory management of supply chains with general network structures. *Comput Chem Eng* **2016,** 87, 164-179.

31. Caballero, J. A.; Grossmann, I. E., An algorithm for the use of surrogate models in modular flowsheet optimization. *Aiche J* **2008,** 54, (10), 2633-2650.

32. Boukouvala, F.; Ierapetritou, M. G., Surrogate-Based Optimization of Expensive Flowsheet Modeling for Continuous Pharmaceutical Manufacturing. *J Pharm Innov* **2013,** 8, (2), 131-145.

33. Cozad, A.; Sahinidis, N. V.; Miller, D. C., Learning surrogate models for simulation-based optimization. *Aiche J* **2014,** 60, (6), 2211-2227.

34. Yee, T. F.; Grossmann, I. E., Simultaneous optimization models for heat integration—II. Heat exchanger network synthesis. *Comput Chem Eng* **1990,** 14, (10), 1165-1184.

35. Ahmetović, E.; Ibrić, N.; Kravanja, Z.; Grossmann, I. E., Water and energy integration: A comprehensive literature review of non-isothermal water network synthesis. *Comput Chem Eng* **2015,** 82, 144-171.

36. Biegler, L. T.; Grossmann, I. E.; Westerberg, A. W., *Systematic methods for chemical process design*. Prentice Hall, Old Tappan, NJ (United States): United States, 1997.

37. Floudas, C. A.; Niziolek, A. M.; Onel, O.; Matthews, L. R., Multi-scale systems engineering for energy and the environment: Challenges and opportunities. *Aiche J* **2016,** 62, (3), 602-623.

38. Biegler, L. T., New Nonlinear Programming Paradigms for the Future of Process Optimization.

Aiche J **2017,** 63, (4), 1178-1193.

39. Gao, M.; Sun, F. Z.; Zhou, S. J.; Shi, Y. T.; Zhao, Y. B.; Wang, N. H., Performance prediction of wet cooling tower using artificial neural network under cross-wind conditions. *Int J Therm Sci* **2009,** 48, (3), 583-589.

40. Wei, X. Q.; Li, N. P.; Peng, J. Q.; Cheng, J. L.; Hu, J. H.; Wang, M., Performance Analyses of Counter-Flow Closed Wet Cooling Towers Based on a Simplified Calculation Method. *Energies* **2017,** 10, (3).

41. Qasim, S. M.; Hayder, M. J., Parametric study of closed wet cooling tower thermal performance. *Iop Conf Ser-Mat Sci* **2017,** 227.

42. Apte, S. V.; Gorokhovski, M.; Moin, P., LES of atomizing spray with stochastic modeling of secondary breakup. *Int J Multiphas Flow* **2003,** 29, (9), 1503-1522.

43. Pawar, S. K.; Abrahams, R. H. M.; Deen, N. G.; Padding, J. T.; van der Gulik, G. J.; Jongsma, A.; Innings, F.; Kuipers, J. A. M., An Experimental Study Of Dynamic Jet Behaviour In a Scaled Cold Flow Spray Dryer Model Using Piv. *Can J Chem Eng* **2014,** 92, (12), 2013-2020.

44. Pawar, S.; Padding, J.; Deen, N.; Jongsma, A.; Innings, F.; Kuipers, J. A. M., Numerical and experimental investigation of induced flow and droplet-droplet interactions in a liquid spray. *Chem Eng Sci* **2015,** 138, 17-30.

45. Bazdidi-Tehrani, F.; Zeinivand, H., Presumed PDF modeling of reactive two-phase flow in a three dimensional jet-stabilized model combustor. *Energ Convers Manage* **2010,** 51, (1), 225-234.

46. Chen, H.; Yang, C.; Deng, K. J.; Zhou, N. N.; Wu, H. C., Multi-objective optimization of the hybrid wind/solar/fuel cell distributed generation system using Hammersley Sequence Sampling. *Int J Hydrogen Energ* **2017,** 42, (12), 7836-7846.

47. Salazar, J. M.; Diwekar, U. M.; Zitney, S. E., Stochastic Simulation of Pulverized Coal (PC) Processes. *Energ Fuel* **2010,** 24, (9), 4961-4970.

48. Iman, R. L.; Conover, W. J., A distribution-free approach to inducing rank correlation among input variables. *Communications in Statistics - Simulation and Computation* **1982,** 11, (3), 311-334.

49. Duran, M. A.; Grossmann, I. E., An outer-approximation algorithm for a class of mixed-integer nonlinear programs. *Math Program* **1986,** 36, (3), 307-339.